



UNIVERSITY
OF TRENTO

DIPARTIMENTO DI INGEGNERIA E SCIENZA DELL'INFORMAZIONE

38123 Povo – Trento (Italy), Via Sommarive 14
<http://www.disi.unitn.it>

AN INNOVATIVE MULTI-RESOLUTION APPROACH FOR DOA
ESTIMATION BASED ON A SUPPORT VECTOR CLASSIFICATION

Donelli, F. Viani, P. Rocca, and A. Massa

January 2011

Technical Report # DISI-11-027

An Innovative Multi-Resolution Approach for DOA Estimation based on a Support Vector Classification

M. Donelli, F. Viani, P. Rocca, and A. Massa

Department of Information and Communication Technology,
University of Trento, Via Sommarive 14, 38050 Trento - Italy
Tel. +39 0461 882057, Fax +39 0461 882093

E-mail: *andrea.massa@ing.unitn.it*,

{massimo.donelli, federico.viani, paolo.rocca}@dit.unitn.it

Web-site: *http://www.eledia.ing.unitn.it*

An Innovative Multi-Resolution Approach for DOA Estimation based on a Support Vector Classification

M. Donelli, F. Viani, P. Rocca, and A. Massa

Abstract

The knowledge of the directions of arrival (*DOAs*) of the signals impinging on an antenna receiver enables the use of adaptive control algorithm suitable for limiting the effects of interferences and increasing the gain towards the desired signals in order to improve the performances of wireless communication systems. In this paper, an innovative multi-resolution approach for the real-time *DOA* estimation of multiple signals impinging on a planar array is presented. The method is based on a support vector classifier and it exploits a multi-scaling procedure to enhance the angular resolution of the detection process in the regions of incidence of the incoming waves. The data acquired from the array sensors are iteratively processed with a support vector machine (*SVM*) customized to the problem at hand. The final result is the definition of a map of the probability that a signal impinges on the antenna from a fixed angular direction. Selected numerical results, concerned with both single and multiple signals, are provided to assess potentialities and current limitations of the proposed approach.

Key words: Planar Arrays, *DOA* Estimation, Classification, Multi-Resolution, Support Vector Machine.

1 Introduction

In the last decades, the technology of adaptive antenna arrays has been greatly advanced and applied to many mobile and wireless communication systems [1][2]. Within this framework, the antenna beam-forming plays an important role and the estimation of the directions of arrival (*DOAs*) of signals impinging on the array is a crucial task in order to enhance the spatial diversity and consequently the spectral efficiency. As a matter of fact, such an information enables the generation or steering of the radiation pattern with a maximum towards the desired signals and nulls along the directions of interfering signals [3][4]. The effects of interferences are mitigated and both the gain and the performance of the whole communication system are enhanced. For such reasons, the estimation of the *DOAs* of unknown interfering and desired signals is of great interest and it is still an open problem as confirmed by the number of papers published on this topic.

In the scientific literature, several methods have been proposed for the direction finding of multiple signals impinging on an array of narrow band sensors. Among them, the most widely known and used are *ESPRIT* (Estimation of Signal Parameters via Rotational Invariance Technique) [5]-[7] and *MUSIC* (MUltiple SIgnal Classification) [8][9]. Other approaches based on the maximum likelihood (*ML*) *DOA* estimation have been proposed [10][11], as well.

In the last years, great attention has been also paid to the use of learning-by-examples (*LBE*) techniques. *LBE*-based approaches are able to provide a good trade-off between accuracy and convergence, which is mandatory for real time systems where fast reactions are required. Furthermore, they satisfactorily deal with unknown configurations (i.e., different from those “learned” during the training process) thanks to their generalization capability. Within this framework, the benefits of using radial basis function neural networks (*RBFNN*) have been carefully analyzed in [12]. As a matter of fact, neural networks (*NNs*) are suitable in approximating non-linear functions as those in *DOAs* estimation. Moreover, they can be easily implemented in analog circuits. An improved *RBFNN*-based approach has been presented by the same authors of [12] in [13] to address the problem of tracking an unknown number of multiple sources when no *a-priori* information on the number of impinging signals is available. More specifically, the region above the antenna has been partitioned into angular sectors and each

sector “assigned” to a simpler NN , thus reducing with respect to [12] the problem complexity as well as the computational burden of the learning phase. Towards this end, each network has been trained to detect the subset of incoming signals that impinge on the corresponding angular sector. Accordingly, only those NN s of the regions where the signals have been detected in the first stage of the process are activated in the second one to estimate the $DOAs$ of the incoming signals.

More recently, some techniques based on support vector machines ($SVMs$) [14] have been analyzed to profitably exploit their solid mathematical foundation in statistical learning theory [15]. The main advantages of those approaches lie in their ability to deal with various and complex electromagnetic problems [16][17], and, analogously to NNs , in an easy hardware implementation [18]. As far as the DOA estimation is concerned, a support vector regression (SVR) procedure has been presented in [19] when dealing with linear arrays. In such a case, a SVM has been used to estimate the DOA of each impinging electromagnetic wave starting from a set of known input-output examples where the $DOAs$ of the signals were uniformly distributed in the whole angular region above the receiver. Despite the generalization capability of the SVR -based method, an *a-priori* information on the number of sources and pre-fixed angular separations between the $DOAs$ (as in [12]) have been considered to increase the reliability of the estimation procedure. An extension of such a model has been presented in [20] and experimentally validated in [21] successively.

In this paper, an innovative procedure for real-time direction finding of signals impinging on a planar array of electromagnetic sensors is presented. The problem of the $DOAs$ estimation is formulated as a two step procedure, where the first step is aimed at determining the decision function that correctly classifies whatever input pattern by means of a SVM -based approach. In the second step, the output of the decision function is mapped into the *a-posteriori* probability that a signal impinges on the antenna from a fixed direction. In order to increase the accuracy of the estimation process and to reduce the computational burden affecting other $DOAs$ procedures, the proposed two-step strategy is nested into an iterative multi-scaling process [22]. Accordingly, the resolution accuracy is improved only in those angular regions where the unknown sources are supposed to be located at the previous iteration. More specifically, the algo-

rithm first determines a coarse probability map of the *DOAs* starting from a training set where the incoming signals are non-uniformly distributed along the elevation direction, θ , and the azimuthal one, ϕ . Then, the *SVM* is used to classify the input test dataset at successive resolution levels by performing a kind of synthetic zoom in the angular regions of interest (*ARoIs*) where a higher probability is detected and considering the same training set, thus performed only once and off-line. Concerning the antenna architecture and unlike [13] and [20], planar arrays of sensors are considered since linear arrays lack the ability to scan in *3D*-space and the estimation of both the elevation θ and the azimuth ϕ angles is crucial and has many applications in various fields of engineering. For instance, a complete *DOA* information it is possible to improve the coverage of transmission in wireless communications by avoiding interferences and enhancing the system capacity [23]. More specifically, planar arrangements are very attractive in mobile communications with portable devices where the main beam must be scanned in any direction [24]. Moreover, the number of impinging signals is unknown as well as their directions belonging to the whole angular range above the planar antenna system (i.e., $\theta \in [0 : 90^\circ]$ and $\phi \in [0 : 360^\circ]$).

The paper is organized as follows. The formulation of the iterative two-step multi-resolution *DOA* approach (in the following denoted by the acronym *IMSA – SVM*) is described in Section 2. In order to show the innovative features of the approach and to assess its effectiveness, a selected set of numerical results concerned with both single and multiple signals is reported and discussed (Sect. 3). Moreover, some comparisons with state-of-the-art techniques are also reported. Finally, some conclusions are drawn in Sect. 4.

2 Mathematical Formulation

Let us consider a planar array of M isotropic elements displaced on a regular and rectangular grid with inter-element spacing d on the $x - y$ plane. A set of I electromagnetic waves impinge on the array from unknown angular directions (θ_i, ϕ_i) , $i = 1, \dots, I$, as sketched in Fig. 1. The signals, supposed to be narrow-band and centered at the carrier frequency f (λ being the corresponding free-space wavelength), are generated by a set of electromagnetic sources placed in the far-field of the receiving antenna. The open-circuit voltage at the output of the m -th

sensor can be expressed as [20]

$$v_m = \sum_{i=1}^I \{a_m(\theta_i, \phi_i) [\underline{E}_i(x_m, y_m) \cdot \underline{e}_m]\} + g_m, \quad m = 1, \dots, M \quad (1)$$

where $a_m(\theta_i, \phi_i) = e^{j\frac{2\pi}{\lambda} \sin\theta_i(x_m \cos\phi_i + y_m \sin\phi_i)}$, (x_m, y_m) being the location of the m -th sensor expressed in wavelength, and g_m is the background random noise at the m -th locations. The noise samples are supposed to be statistically independent and characterized by a random Gaussian distribution with zero mean value. Moreover, \underline{E}_i and \underline{e}_m are the electric field associated to the i -th impinging wave and the effective length of the m -th array element.

According to the guidelines described in [3] and [4] about the control of adaptive/smart antennas, the solution of the *DOAs* estimation problem is based also in this work on the measurement of the total correlation matrix, defined as

$$\underline{\Phi} = E \{ \underline{v} \cdot \underline{v}^* \} \quad (2)$$

where $\underline{v} = \{v_m; m = 1, \dots, M\}$ and the superscript $*$ stands for complex conjugation, at the output of the planar array since it contains sufficient information on the received signals [13].

From a statistical point of view, the problem at hand can be formulated as the definition of the probability map of the angular incidence of the incoming waves starting from the knowledge of the total correlation matrix $\underline{\Phi}$. Towards this end, let us partition the angular region above the array into a two-dimensional lattice of $H = H_\theta \times H_\phi$ cells, each one corresponding to an angular sector of sides $\Delta\theta$ and $\Delta\phi$ [Fig. 2(a)]. The status χ_h of each cell can be *empty* [$\chi_h = \chi(\theta_h, \phi_h) = -1$], if any signal impinges on the array from the angular region identified by the same cell, or *occupied* [$\chi_h = \chi(\theta_h, \phi_h) = 1$], otherwise. Accordingly, the original problem can be stated as follows: “*find the a-posteriori probability function $Q(\theta, \phi)$ given a measured value of the total correlation matrix $\underline{\Phi}$ at the receiver*”. Mathematically, $Q(\theta, \phi)$ can be also expressed as the linear combination of the non-overlapping basis functions $B_h(\theta, \phi)$, $h = 1, \dots, H$ defined over the angular lattice

$$Q(\theta, \phi) = \sum_{h=1}^H q(\theta_h, \phi_h) B_h(\theta, \phi) \quad (3)$$

where the weighting coefficient $q(\theta_h, \phi_h)$ is the probability value that a wave impinges on the array from the h -th angular sector [i.e., $q(\theta_h, \phi_h) = Pr\{\chi_h = 1; \underline{\Phi}\}$] and $B_h(\theta, \phi) = 1$ if (θ, ϕ) belongs to the h -th cell and $B_h(\theta, \phi) = 0$ otherwise.

In order to improve the achievable angular resolution, a multi-resolution representation of the unknown function $Q(\theta, \phi)$ is looked for [Fig. 2(b) - $r = 1$] by exploiting an iterative process analogously to [22]. More specifically, the probability function is expressed at the s -th step of the iterative procedure as a twofold summation of shifted and dilated spatial basis functions

$$Q^{(s)}(\theta, \phi) = \sum_{r=0}^{R(s)} \sum_{h(r)=1}^{H(r)} q^{(s)}(\theta_{h(r)}, \phi_{h(r)}) B_{h(r)}(\theta, \phi); s = 1, \dots, S_{opt} \quad (4)$$

r being the resolution index and $R(s) = s - 1$. The summation over r ranges from 0 [Fig. 2(a)], which corresponds to the largest characteristic length scale, to $R(s)$ [Fig. 2(b)], which corresponds to the smallest angular basis-function support at the s -th scaling step. For a given value of r , $H(r) = H_\theta^{(r)} \times H_\phi^{(r)}$ is the number of non-overlapped basis functions centered in the angular sub-domain represented at the r -th resolution. Accordingly, the iterative *DOA* detection procedure is aimed at locating the terms of small length scale at those *ARoIs* [e.g., the yellow cells in Figs. 2(a)-2(b)] where the signals are supposed to impinge with higher probability.

In order to profitably exploit the multiresolution representation of the *a-posteriori* probability function (4) and solving the arising *DOA* problem, the following multistep classification process is performed by means of a *SVM*-based technique. More in detail,

- **Step 0 - SVM Training Phase.** The *SVM* is trained once and off-line starting from the knowledge of a set of known examples (i.e, input/output relationships)

$$\left\{ \left[\underline{\Phi}, (\theta_n, \phi_n), \chi_n = \chi(\theta_n, \phi_n); n = 1, \dots, N \right]^{(t)}; t = 1, \dots, T \right\} \quad (5)$$

called *training set*, where T is the number of training data. The N samples of each training data are composed by $I(t)$ examples concerned with angular positions (θ_i, ϕ_i) , $i = 1, \dots, I(t)$, $I(t) \leq I_{max}$ where a signal impinges on the array [i.e., *occupied* directions - $\chi(\theta_i, \phi_i) = 1; i = 1, \dots, I(t)$], while the remaining $F(t) = N - I(t)$ are related to

empty directions [i.e., $\chi(\theta_f, \phi_f) = -1; f = 1, \dots, F(t)$].

Starting from the knowledge of the *training set*, the problem turns out to be the definition of a suitable discriminant function $\hat{\mathcal{S}}$

$$\hat{\mathcal{S}} : \underline{\Phi} \rightarrow [\chi(\theta_h, \phi_h); h = 1, \dots, H] \quad (6)$$

that separates the two classes $\chi(\theta, \phi) = 1$ and $\chi(\theta, \phi) = -1$ on the basis of the total correlation matrix $\underline{\Phi}$ measured at the output of the planar array. In order to approach the problem with a single classifier, the problem at hand is reformulated as that of building the following single output function

$$\hat{\mathcal{S}} : [\underline{\Phi}, (\theta_n, \phi_n); n = 1, \dots, N] \rightarrow \chi(\theta_h, \phi_h), \quad h = 1, \dots, H. \quad (7)$$

Towards this purpose and according to the *SVM* theory [15], the following linear decision function is adopted

$$\hat{\mathcal{S}} \{ \underline{\varphi}(\underline{\Phi}, (\theta_n, \phi_n)) \} = \underline{w} \cdot \underline{\varphi}(\underline{\Phi}, (\theta_n, \phi_n)) + b, \quad n = 1, \dots, N. \quad (8)$$

$\hat{\mathcal{S}}$ is determined in a space (called “*feature space*”) with a higher dimensionality than the original input data space and obtained through the non-linear operator $\underline{\varphi}(\cdot)$ [15]. The unknown terms \underline{w} and b , which unequivocally define the decision hyperplane $\hat{\mathcal{S}}$, are the normal vector and a bias, respectively. They are computed during the *Training Phase* according to the guidelines described in [17];

- **Step 1 - Low-Order DOA Estimation** ($s = 1$). At the first step, a coarse probability map [Eq. (4) - $s = 1$] is determined by means of the *SVM* classifier mapping the decision function $\hat{\mathcal{S}}$ into the *a-posteriori* probability function.

The unknown probability coefficients $q^{(s)}(\theta_h, \phi_h) \Big|_{s=1}, h = 1, \dots, H$ are approximated with a sigmoid function [15] as follows

$$q^{(s)}(\theta_h, \phi_h) = \frac{1}{1 + \exp\left[\gamma \hat{\mathfrak{S}}\left\{\underline{\varphi}(\underline{\Phi}, (\theta_h, \phi_h))\right\} + \nu\right]} \quad (9)$$

where γ and ν are two parameters computed according to a fitting process [17] starting from a subset of the T training data of the *Training Set*;

- **Step 2** - *IMSA – SVM Process* ($s \geq 1$).

- **Step 2.a** - *Angular Regions of Interest (ARoIs) Identification* ($s \leftarrow s + 1$). Starting from the probability map previously (i.e., at the $s - 1$ -th iteration) determined, such a step is aimed at identifying the angular sectors $D_\ell^{(s)}$, $\ell = 1, \dots, L(s)$ where the signals are supposed to impinge in order to improve the resolution only in those regions and enhance the accuracy of the *DOA* estimation. Towards this end, first the values of the function $Q^{(s-1)}(\theta, \phi)$ are scaled, thus defining the following new set of normalized probability coefficients

$$p^{(s-1)}(\theta_{h(r)}, \phi_{h(r)}) = \frac{q^{(s-1)}(\theta_{h(r)}, \phi_{h(r)})}{q_M - q_m} + \frac{q_m}{q_m - q_M}, \quad \begin{array}{l} h(r) = 1, \dots, H(r) \\ r = 0, \dots, R(s) \end{array} \quad (10)$$

where $q_M = \max_{r=0, \dots, R(s)} \left\{ \max_{h(r)=1, \dots, H(r)} [q^{(s-1)}(\theta_{h(r)}, \phi_{h(r)})] \right\}$ and $q_m = \min_{r=0, \dots, R(s)} \left\{ \min_{h(r)=1, \dots, H(r)} [q^{(s-1)}(\theta_{h(r)}, \phi_{h(r)})] \right\}$. Successively, the new probability function

$$P^{(s-1)}(\theta, \phi) = \sum_{r=0}^{R(s-1)} \sum_{h(r)=1}^{H(r)} p^{(s-1)}(\theta_{h(r)}, \phi_{h(r)}) B_{h(r)}(\theta, \phi)$$

is thresholded by nulling the scaled coefficients greater than a user-defined threshold η . Finally, the thresholded function

$$P_{th}^{(s-1)}(\theta, \phi) = \sum_{r=0}^{R(s-1)} \sum_{h(r)=1}^{H(r)} p_{th}(\theta_{h(r)}, \phi_{h(r)}) B_{h(r)}(\theta, \phi) \quad (11)$$

where $p_{th}(\theta_{h(r)}, \phi_{h(r)}) = p^{(s-1)}(\theta_{h(r)}, \phi_{h(r)})$ if $p^{(s-1)}(\theta_{h(r)}, \phi_{h(r)}) > \eta$ and $p_{th}(\theta_{h(r)}, \phi_{h(r)}) =$

0 otherwise, allows one to identify the *ARoIs*, $D_\ell^{(s)}$, $\ell = 1, \dots, L(s)$ defined as those angular sub-domains where $P_{th}^{(s-1)}(\theta, \phi) \neq 0$;

- **Step 2.b** - *Multiresolution DOA Estimation*. A synthetic zoom is performed by refining the representation of the unknown function $Q^{(s)}(\theta, \phi)$ and increasing the angular resolution ($r \leftarrow r + 1$) only in the *ARoIs* identified at (*Step 2.a*). Therefore, the multiresolution *a-posteriori* probability function (4) is updated⁽¹⁾ by setting $Q^{(s)}(\theta, \phi) = P_{th}^{(s-1)}(\theta, \phi)$ and computing the new highest resolution coefficients, $q^{(s)}(\theta_{h(r)}, \phi_{h(r)})$, when $(\theta, \phi) \in D_\ell^{(s)}$, $\ell = 1, \dots, L(s)$ as in (9);
- **Step 3** - *Termination Criterion* ($s = S_{opt}$). The sequence of operations of *Step 2* is repeated until both the dimensions and the number of *ARoIs* between two consecutive cycles are stationary [i.e., $L(s) = L(s - 1)$ and the variations of the dimensions of the *ARoIs* are not greater than the highest angular resolution at the s -th step, $\Delta_{min}^{(s)} = \min \{ \Delta\theta_{R(s)}^{(s)}, \Delta\phi_{R(s)}^{(s)} \}$].

3 Numerical Simulations and Results

In order to assess the effectiveness and reliability of the proposed approach, an exhaustive set of numerical experiments has been performed and some selected results will be reported in the following for illustrative purposes. The remaining of this section will firstly (Sect. 3.1) illustrate the behavior of the multi-scaling procedure also in comparison with other state-of-the-art approaches for *DOA* estimation. The second part (Sect. 3.2) will be devoted to analyze the potentialities and current limitations of the *IMSA – SVM* approach when dealing with various and challenging electromagnetic scenarios. In such a framework, some configurations in which conventional state-of-the-art signal subspace-based array processing techniques cannot be applied are also dealt with in order to point out the enhanced range of applicability of *SVM* approaches. Finally, a uniform array of $\frac{\lambda}{2}$ -dipoles is considered (Sect. 3.3) to verify the suitability and reliability of the proposed method in correspondence with a realistic array modelling.

⁽¹⁾It is worth noting that at the s -th step of the multi-scaling procedure only the angular ranges belonging to the *ARoIs* are processed by the *SVM* classifier with a non-negligible saving of computational resources.

With reference to the geometry shown in Fig. 1, a square planar array of $M = 16$ isotropic radiators spaced by $d = \frac{\lambda}{2}$ is considered. The power of the impinging signals has been set to $P_i = 30 \text{ dB}$, $i = 1, \dots, I$ above the level of the background noise.

Concerning the training set, the following setup $T = 400$ and $I_{max} = 4$ has been assumed and the *SVM* classifier has been trained once and off-line on the same data set whatever the test experiment. As regards to the $T = \sum_{i=1}^{I_{max}} T_i$ training examples, different scenarios have been considered, $T_i = 100$ being the number of configurations with i signals. Moreover, the actual *DOAs* of the signals of the training data have been randomly chosen in a discrete grid of locations (θ_n, ϕ_n) , $n = 1, \dots, N$ belonging to the the angular region above the antenna

$$\begin{cases} \theta_n = \theta_0 + \left\lfloor \frac{n-1}{\sqrt{N}} \right\rfloor \Delta\theta \\ \phi_n = \phi_0 + \left\lceil \frac{n-1}{\sqrt{N}} \right\rceil \Delta\phi \end{cases}, \quad n = 1, \dots, N \quad (12)$$

$\lfloor \cdot \rfloor$ and $\lceil \cdot \rceil$ being the floor function and the ceiling function, respectively. Moreover, in order to fully assess the generalization properties of the *SVM*-based approach, the *DOAs* of the test examples are different from those of the training dataset.

3.1 Single Signal Scenario - Comparative Assessment

The first experiment deals with the *DoA* detection of a single signal and a *test set* of $T_1^{(test)} = 100$ examples related to the single-signal scenario has been considered. An illustrative description of the behavior of the proposed *IMSA – SVM* approach is shown in Fig. 3 dealing with the “representative” (of the method performance on the whole test dataset) configuration of a signal coming from $(\theta_1 = 53^\circ, \phi_1 = 260^\circ)$. At the first step ($s = 1$), the planar angular region $D^{(1)}$ is partitioned into $H^{(s)} = 81$ cells (being $\Delta\theta_{(r)}^{(s)} = 10^\circ$ and $\Delta\phi_{(r)}^{(s)} = 40^\circ$, $r = 0$, the angular steps along the elevation direction, θ , and the azimuthal one, ϕ , respectively) and a coarse *DOA* probability map is determined following the procedure described in Sect. 2 (*Step 1*). Then, the multi-scaling procedure takes place ($s \geq 2$). The *ARoIs* are identified and partitioned into $H_{R^{(s)}}^{(2)} \Big|_{R^{(s)}=s-1} = 81$ cells with an angular resolution of $\Delta\theta_{(1)}^{(2)} = 5^\circ$ and $\Delta\phi_{(1)}^{(2)} = 20^\circ$. For the sake of space, only the *DOA* probability map obtained at the end of the second step ($s = 2$)

is shown in Fig. 3(a). The procedure is then iterated until $s = S_{opt} = 4$ [$R(S_{opt}) = 3$] with the final result reported in Fig. 3(b) characterized by an angular resolution in $D_1^{(4)}$ equal to $\Delta\theta_{(3)}^{(4)} = 1.25^\circ$ and $\Delta\phi_{(3)}^{(4)} = 5^\circ$. As it can be observed (Fig. 3), the region with higher probability of incidence turns out to be closer and closer to the actual angular location of the signal when increasing the step number. Quantitatively such an event can be analytically quantified by computing the values of the *location index* $\zeta^{(s)}$ (Fig. 1) and of the *incidence area* $\psi^{(s)}$ defined as follows

$$\zeta^{(s)} = \frac{\Phi^{(s)}}{\max\{\Phi^{(s)}\}} \times 100 \quad (13)$$

where $\Phi^{(s)} \triangleq \sqrt{\left(\sin\theta\cos\phi - \sin\hat{\theta}^{(s)}\cos\hat{\phi}^{(s)}\right)^2 + \left(\sin\theta\sin\phi - \sin\hat{\theta}^{(s)}\sin\hat{\phi}^{(s)}\right)^2 + \left(\cos\theta - \cos\hat{\theta}^{(s)}\right)^2}$ and

$$\psi^{(s)} = \pi \left\{ \frac{\sum_{r=0}^{R(s)} \sum_{h(r)=1}^{H(r)} \left\{ \frac{\zeta_{h(r)}^{(s)} q^{(s)}(\theta_{h(r)}, \phi_{h(r)})}{\max_{h(r)}\{q^{(s)}(\theta_{h(r)}, \phi_{h(r)})\}} \right\}}{\sum_{r=0}^{R(s)} \sum_{h(r)=1}^{H(r)} \left\{ \frac{q^{(s)}(\theta_{h(r)}, \phi_{h(r)})}{\max_{h(r)}\{q^{(s)}(\theta_{h(r)}, \phi_{h(r)})\}} \right\}} \right\}^2 \quad (14)$$

being $\zeta_{h(r)}^{(s)} = \left[\left(\sin\theta_{h(r)}\cos\phi_{h(r)} - \sin\hat{\theta}^{(s)}\cos\hat{\phi}^{(s)}\right)^2 + \left(\sin\theta_{h(r)}\sin\phi_{h(r)} - \sin\hat{\theta}^{(s)}\sin\hat{\phi}^{(s)}\right)^2 + \left(\cos\theta_{h(r)} - \cos\hat{\theta}^{(s)}\right)^2 \right]^{\frac{1}{2}}$, (θ, ϕ) are the actual coordinates of the signal incidence point, whereas $(\hat{\theta}, \hat{\phi})$

$$\hat{\theta}^{(s)} = \frac{\sum_{r=0}^{R(s)} \sum_{h(r)=1}^{H(r)} \{\theta_{h(r)} q^{(s)}(\theta_{h(r)}, \phi_{h(r)})\}}{\sum_{r=0}^{R(s)} \sum_{h(r)=1}^{H(r)} \{q^{(s)}(\theta_{h(r)}, \phi_{h(r)})\}} \quad \hat{\phi}^{(s)} = \frac{\sum_{r=0}^{R(s)} \sum_{h(r)=1}^{H(r)} \{\phi_{h(r)} q^{(s)}(\theta_{h(r)}, \phi_{h(r)})\}}{\sum_{r=0}^{R(s)} \sum_{h(r)=1}^{H(r)} \{q^{(s)}(\theta_{h(r)}, \phi_{h(r)})\}} \quad (15)$$

identify the center of the ℓ -th *ARoI* where the signal/signals is/are supposed to impinge. As a matter of fact, the value of the location index reduces from $\zeta^{(1)} = 13.17$ down to $\zeta^{(S_{opt})} = 2.53$ (being $\zeta^{(2)} = 4.10$ and $\zeta^{(3)} = 2.87$). Analogously, $\psi^{(1)} = 2.74$, $\psi^{(2)} = 0.94$, $\psi^{(3)} = 0.36$, until $\psi^{(S_{opt})} = 0.14$. As regards to the whole set of test examples, the statistics of the “convergence” values of the indexes (13) and (14) are given in the first block of Tab. I.

In order to get an insight into the advantages of the proposed multi-resolution approach over the classification single-step techniques, a bare *DOA SVM*-based method has been considered and applied to the same test example. To fairly compare the two methods, the same training dataset has been used. Moreover, the same angular resolution has been adopted in both cases. Towards

this purpose, an angular lattice characterized by a uniform grid whose cell side was equal to the finest discretization of the multi-resolution procedure (i.e., $\Delta\theta = \Delta\theta_{(3)}^{(4)}$ and $\Delta\phi = \Delta\phi_{(3)}^{(4)}$), has been defined over the whole angular investigation domain of the single step *SVM* approach. As it can be observed [Fig. 4(a)], although the value of ς is quite close to that of the *IMSA* strategy (i.e., $\varsigma]_{IMSA-SVM} = 2.53$ vs. $\varsigma]_{SVM} = 3.14$), the extension of the incidence area turns out to be significantly wider ($\psi]_{IMSA-SVM} = 0.14$ vs. $\psi]_{SVM} = 2.79$). On the other hand, it cannot be neglected that the *CPU*-time of the test phase of the bare procedure is approximately fifty times the one of the *IMSA – SVM* because of the need to obtain a detailed map in the whole investigation area $D_1^{(1)}$ instead of in a limited *ARoI*, $D_1^{(S_{opt})}$, only. As a matter of fact, the number of test points used by the *IMSA* approach turns out to be widely reduced.

For completeness, the results from other standard nonlinear classification methods, such as the multilayer perceptron (*MLP*) and the radial basis functions (*RBF*) neural network, have been analyzed, as well. More specifically, the *DOA* probability maps obtained with the *MLP*-based and *RBFNN*-based classifiers are reported in Figs. 4(b) and 4(c), respectively. Whatever the method, the achieved estimate does not appear to be adequate and certainly not comparable neither with that of the *IMSA – SVM* [Figs. 4(b)-4(c) vs. Fig. 3(b)] nor with that of the bare *SVM* [Figs. 4(b)-4(c) vs. Fig. 4(a)] as also confirmed by the values of the location index: $\varsigma]_{RBF} = 10.21$ and $\varsigma]_{MLP} = 25.91$.

The last analysis is concerned with the comparison between the *IMSA – SVM* and those state-of-the-art methods for *DOA* estimation aimed at determining the angular incidence of the signals, namely *MUSIC*, *ESPRIT* (i.e., two one-dimensional *ESPRIT*'s independently-applied to the arrays followed by an alignment procedure to associate the estimated azimuth and elevation angle), *2D-unitary ESPRIT* [7], and a support vector regression-based (*SVR*) approach. Towards this end, the azimuthal direction of the actual signal has been fixed to $\phi = 260^\circ$, while the elevation angle has been varied in the range $\theta \in [20^\circ \div 80^\circ]$. Moreover, the *SVR* algorithm has been previously trained with a dataset composed by $T = T_1 = 100$ examples concerned with only one signal ($I = 1$). The methods are then compared by means of the resulting signal location error, ς .

Because of the planar array of isotropic elements and as expected [25], the performances of the

DOA techniques in θ elevation-estimation turn out to be better at high elevations ($\theta \rightarrow 0^\circ$) [Tab. II], while the ϕ azimuth-estimation is greatest at low elevations ($\theta \rightarrow 90^\circ$). Moreover, the values of the estimation indexes point out that the *IMSA – SVM* (last column - Tab. II) is able to obtain similar results, in terms of angular resolution, than those provided by the *SVR* and of the same order in magnitude of *MUSIC* and *ESPRIT*s except for wider angles ($\theta \geq 60^\circ$), even though these latter need more *CPU*-time (i.e., an optimized *IMSA – SVM* implementation just needs few milliseconds on a *PC* equipped with a 3.0 *GHz* processor and 2 *GHz* of *RAM*). As regards to the growing of the location index around 60° , it mainly depends on the training set. As a matter of fact, it can be avoided by modifying the off-line training phase. For instance, the choice of a uniform angular distribution of the training samples (Fig. 5), instead of a non-uniform arrangement, allows one to obtain a behavior of ζ almost invariant to θ for medium-high elevations.

In order to point out the generalization capabilities of the proposed approach as well as its robustness to the model tolerances [14][26], the effect of the array failure has been evaluated and the arising results compared to those with *2D-unitary ESPRIT* which demonstrated several advantages over *MUSIC* and the standard *ESPRIT* implementation. Towards this end, an increasing number of array elements has been switched off. Moreover, the *a-priori* information on the failure of some array elements has not been exploited through the definition of an ad-hoc training set, but the same non-uniform set of input-output examples concerned with the unperturbed array structure has been used. The results of the comparative assessment when ($\theta_1 = 53^\circ$, $\phi_1 = 260^\circ$) are reported in Fig. 6.

3.2 Complex Scenarios - Performance Analysis

The following experiments are aimed at assessing the effectiveness of the *IMSA – SVM* in detecting the *DOAs* of multiple signals.

Dealing with the detection of two different incidence points, the first example is concerned with test signals coming from ($\theta_1 = 12^\circ$, $\phi_1 = 165^\circ$) and ($\theta_2 = 82^\circ$, $\phi_2 = 165^\circ$), respectively. The probability maps estimated by the *IMSA – SVM* at different steps are shown in Fig. 7 together with those obtained with the single-step *SVM* classification procedure [Fig. 7(d)], the *MLP*-

based approach [Fig. 7(e)], and the *RBF* technique [Fig. 7(f)]. As expected and confirming the outcomes from the study of the single-signal detection, the multi-scaling process allows one to significantly enhance the performances of the single-step classification approaches as pictorially shown in Fig. 7 and quantitatively confirmed by the indexes in Tab. III. Moreover, it is worth noting that this conclusion is not limited to a particular configuration of incidence angles, but it holds true whatever the two-signals scenario under test.

In order to assess the stability of the proposed approach, a test set composed by $T_2^{(test)} = 100$ examples has been considered. The results obtained with the *IMSA – SVM* are summarized in Tab. I (second block). As expected, the mean values of the averaged performance indexes ($\hat{\zeta}_I \triangleq \sum_{i=1}^I \zeta^{(i)}$ and $\hat{\psi}_I \triangleq \sum_{i=1}^I \psi^{(i)}$) turn out to be very close to those of the previous test example [i.e., $avg(\hat{\zeta}_2) = 4.51$, $avg(\hat{\psi}_2) = 0.28$ versus $\zeta_1^{(S_{opt})} = 4.55$, $\psi_1^{(S_{opt})} = 0.23$ and $\zeta_2^{(S_{opt})} = 3.90$, $\psi_2^{(S_{opt})} = 0.25$].

The second numerical experiment, concerned with multiple incidences, considers three-signals configurations. As regards to the results for a test set of $T_3^{(test)} = 50$ three-signals examples, the values in the third block of Tab. I indicate that the resolution accuracy of the proposed approach does not significantly reduce with respect to the single-signal or two-signals scenarios [$avg(\hat{\zeta}_3) = 5.55$, $avg(\hat{\psi}_3) = 0.15$ vs. $avg(\hat{\zeta}_2) = 4.51$, $avg(\hat{\psi}_2) = 0.28$ and $\hat{\zeta}_1 = 2.81$, $\hat{\psi}_1 = 0.25$]. As an illustrative example, let us consider the case of a set of signals impinging on the array from $(\theta_1 = 8^\circ, \phi_1 = 85^\circ)$, $(\theta_2 = 68^\circ, \phi_2 = 95^\circ)$, $(\theta_3 = 55^\circ, \phi_3 = 290^\circ)$. Starting from the coarse map determined, three different *ARoIs* are successively identified [Fig. 8(a)] and better resolved thus iteratively improving the *DOA* resolution accuracy as pointed out by the indexes in Tab. IV where the values estimated by the other classification approaches are reported [Fig. 8(b)], as well. By comparing the distribution at the S_{opt} -th step of the *IMSA* and the one from the bare *SVM*, it is evident the improvement guaranteed by the multi-scaling process both in resolving and properly locating a number of *ARoIs* equal to the number of signals (I).

In the third experiment, $I = 4$ ($I = I_{max}$) signals impinge on the planar array. Figure 9 shows the results provided by the *IMSA – SVM* and in correspondence with a set of representative examples. More in detail, the first example (*Configuration* 1/1/1/1) refers to a configuration

where four separated signals can be recognized $[(\theta_1 = 35^\circ, \phi_1 = 35^\circ), (\theta_2 = 20^\circ, \phi_2 = 115^\circ), (\theta_3 = 70^\circ, \phi_3 = 135^\circ), (\theta_4 = 80^\circ, \phi_4 = 260^\circ)]$ - Figs. 9(a)-9(c)]. The second example [Fig. 9(d)] deals with a two-clusters setup [*Configuration 2/2* - $(\theta_1 = 15^\circ, \phi_1 = 75^\circ), (\theta_2 = 25^\circ, \phi_2 = 120^\circ), (\theta_3 = 75^\circ, \phi_3 = 270^\circ), (\theta_4 = 65^\circ, \phi_4 = 300^\circ)$], while a single signal and a cluster of three-signals are present in the last example [*Configuration 1/3* - $(\theta_1 = 15^\circ, \phi_1 = 105^\circ), (\theta_2 = 80^\circ, \phi_2 = 275^\circ), (\theta_3 = 85^\circ, \phi_3 = 300^\circ), (\theta_4 = 75^\circ, \phi_4 = 315^\circ)$]. Whatever the example, the multi-scaling process is able to identify with an ever increasing resolution from $s = 1$ [Fig. 9(a)] up to $s = S_{opt} = 3$ [Fig. 9(c)] the *ARoIs* to which the incidence directions of the actual signals belong as pointed out by the numerical indexes $\psi^{(i)}, i = 1, \dots, I$ in Tab. V. On the other hand, it should be noticed that the *DOA* estimation process tends to cluster multiple regions-of-incidence in a single *ARoI* when the angular separations among the signals reduce. Such an event takes place also in correspondence with the “*Configuration 2/2*” [Fig. 9(d) - Tab. VI] where two *ARoIs* are identified. It is even more evident in Fig. 9(e) (Tab. VII) where the angular incidences of three signals are detected in only one *ARoI*. The “clustering” effect is quantitatively pointed out by the behavior of the averaged localization index (Tab. I - fourth block) when dealing with the complete test set ($T_4^{(test)} = 50$) to which previous examples belong. As a matter of fact, there is a significant increase of the $avg(\hat{\zeta})$ compared to the values of the same quantity when $I = 1, 2, 3$ [$avg(\hat{\zeta}_4) = 17.29$ vs. $avg(\hat{\zeta}_1) = 2.81, avg(\hat{\zeta}_2) = 4.51, avg(\hat{\zeta}_3) = 5.55$], even though the value of $avg(\hat{\psi})$ remains close to those of other multiple-signals configurations since the estimated *ARoIs* still carefully identify the actual incidence areas.

The fourth and fifth experiments deal with more critical test scenarios since the examples under test are concerned with a number of signals different from that in the training set (i.e., $I \neq 1, 2, 3, 4$). More specifically, let us consider the *Clustered Distribution* of $I = 18$ signals with incidence directions indicated by the white points in Fig. 10. It is worth noticing that such a configuration turns out to be not admissible (i.e., $I = 18$ estimates cannot be obtained) for signal subspace-based array processing techniques as *2D-unitary ESPRIT* when the planar array structure at hand is used. As a matter of fact, the maximum number of sources *2D-unitary*

ESPRIT can handle is equal to [7]

$$I_{max}^{2D ESPRIT} = \min \{U \times (V - 1); V \times (U - 1)\} \quad (16)$$

being $M = U \times V$. On the other hand, it should be considered that an high dimensional array processing is enabled widening the size of the planar array (i.e., the number of array sensors) at the expense of the computational complexity that, unlike *SVM*-based methods, exponentially grows.

Figure 10 compares the “convergence” ($s = S_{opt} = 3$) map provided by the *IMSA – SVM* and the ones from other single-step classifiers. As it can be observed, the multi-scaling process is still able to carefully estimate the *ARoI* to which the actual signals belong with a degree of accuracy higher than that from the other techniques both in terms of localization and area extension (Tab. VIII). Similar conclusions hold true when dealing with the detection of the signals distribution displayed in Fig. 11, although the detection of the single signal on the bottom of the region of analysis appears to be more critical probably because of the absence of similar spatial configurations in the training set.

Finally, the last experiment is concerned with a scenario where there are not signals that impinge on the array and the noise level has been varied from the reference value used for the *SVM* training [$P_n = 20 \text{ dB (Test Set)}$ vs. $P_n = 0 \text{ dB (Training Set)}$] thus further complicating the test case. As a matter of fact, neither the free-case example is present in the training set nor the same noise level has been “learned”. Nonetheless, the *SVM*-based classifier did not detected the presence of any signal thus defining a uniform distribution of probability [Fig. 12(a)]. Otherwise, the other methods give color-maps with some “artifacts” [see Figs. 12(b)-12(c)] although characterized by very small values of the probability of signal incidence.

3.3 Dipole Array Antenna

In the last experiment, a uniform array of $\frac{\lambda}{2}$ -dipoles is taken into account with dipoles oriented along the x axis. Therefore, the effective length [24] of the array element turns out to be

$$\underline{e}_m = \frac{\lambda}{\pi} \left[\frac{\cos\left(\frac{\pi}{2} \sin\theta \cos\phi\right)}{1 - \sin^2\theta \cos^2\phi} \right] [(\cos\theta \cos\phi) \underline{\theta} - (\sin\phi) \underline{\phi}] \quad (17)$$

Moreover, the inter-element distance has been chosen equal to $d_x = 0.65\lambda$ and $d_y = 0.5\lambda$ [27]. Then, a subset of the experiments of the previous sections, but with the dipole array, has been dealt with to evaluate the applicability of the *IMSA – SVM* approach to non-ideal electromagnetic scenarios, as well.

In the first example ($I = 1$), the multi-scaling procedure stops after $S_{opt} = 4$ iterations and the final result is shown in Fig. 13. Likewise the case with point-like sources, the estimations of both the location and the incidence area improve at each iteration starting from $\zeta^{(1)} = 43.19$ and $\psi^{(1)} = 2.48$ down to $\zeta^{(S_{opt})} = 2.96$ and $\psi^{(S_{opt})} = 0.06$, where $\zeta^{(2)} = 12.65$, $\zeta^{(3)} = 5.41$ and $\psi^{(2)} = 0.75$, $\psi^{(3)} = 0.21$. In this case, the performance are comparable to that in Sect. 3.1. Different conclusions arise when processing the data of the two-signal scenario [Fig. 14(a)]. In such a case, only the I_1 (i.e., the signal with the lowest elevation θ) is detected [Fig. 14(a)]. Such an event does not depend on the *DOA* detection method, but from the antenna array at hand. As a matter of fact, the radiation pattern of the array element is omnidirectional in the $z - y$ plane (i.e., $\phi = 90^\circ$ and $\phi = 270^\circ$) with a θ_{3dB} angle of almost 80° degrees [24]. Therefore, the gain of the dipole is lower along the direction with higher θ s, being $\phi_1 = \phi_2 = 165^\circ$. Otherwise, when the actual configuration is described by a set of signals coming from the directions $(\theta_1 = 30^\circ, \phi_1 = 60^\circ)$ and $(\theta_2 = 30^\circ, \phi_2 = 300^\circ)$, the *IMSA – SVM* method still gives accurate estimates [Fig. 14(b)] although with non-ideal isotropic receiving sensors.

4 Conclusions

In this paper, a multi-resolution approach for the *DOA* estimation of multiple signals based on a support vector classifier has been presented. The procedure is aimed at defining a probability map of the incidence of an electromagnetic signal on a planar array of sensors. Starting from a coarse map, a synthetic zoom is iteratively performed in the angular sector where the incidence of a signal has been detected with higher probability at the previous step of the multi-scaling procedure.

The effectiveness of the proposed approach has been assessed dealing with different scenarios and working conditions. Moreover, a comparative analysis has been carried out by considering state-of-the-art *DOA* methods. The obtained results have shown that:

- the use of a classifier based on *SVM* allows one to estimate the *DOA* probability map in real time;
- thanks to the *SVM* generalization capability, the *IMSA – SVM* behaves properly when dealing with complex electromagnetic scenarios non-necessarily belonging to the set of training examples;
- the *SVM*-based approach is able to estimate the *DOAs* of a number of sources greater than the maximum allowed by conventional eigenvalue decomposition methods for a fixed planar array geometry;
- unlike $2 - D$ subspace-based algorithms, the computational complexity does not increase with the size of the rectangular array;
- the proposed *LBE* technique adapts to element failure or other source of errors coming from the tolerances in the array structure that cause non-negligible performance degradation in conventional estimation techniques which require highly calibrated antennas with identical radiation properties;
- the *a-priori* knowledge (deterministic or statistical) on the array configuration and radiation pattern characteristics can be easily and usefully exploited by defining suitable *IMSA – SVM* training sets;
- the multi-scaling procedure (*IMSA*) provides good results dealing with both single-signal and multiple-signals configurations with an angular resolution comparable to that of other state-of-the-art *DOA* algorithms;
- system complexity, classifier architecture, and computational costs significantly reduce with respect to the “bare” classification.

Acknowledgments

The authors wish to thank the reviewers for many valuable suggestions and comments that helped improve this paper. In addition, discussions with Dr. L. Lizzi and Dr. Oliveri are much appreciated.

References

- [1] M. Chryssomallis, "Smart antennas," *IEEE Antennas Propag. Mag.*, vol. 42, no. 3, pp. 129-136, Jun. 2000.
- [2] E. L. Hines, M. S. Leeson, M. M. Ramon, M. Pardo, E. Llobet, D. D. Iliescu, and J. Yang, *Intelligent Systems: Techniques and Applications*. Shaker publishing, 2008.
- [3] S. P. Applebaum, "Adaptive arrays," *IEEE Trans. Antennas Propag.*, vol. 24, no. 5, pp. 585-598, May 1976.
- [4] D. S. Weile and E. Michielssen, "The control of adaptive antenna arrays with genetic algorithms using dominances and diploidy," *IEEE Trans. Antennas Propag.*, vol. 49, no. 10, pp. 1424-1433, Oct. 2003.
- [5] R. Roy and T. Kailath, "ESPRIT-Estimation of signal parameters via rotational invariance techniques," *IEEE Trans. Acust., Speech, Signal Process.*, vol. 37, no. 7, pp. 984-995, Jul. 1989.
- [6] F. Gao and B. Gershman, "A generalized ESPRIT approach to direction-of-arrival estimator," *IEEE Signal Process. Lett.*, vol. 12, no. 3, pp. 254-257, Mar. 2005.
- [7] M. D. Zoltowski, M. Haardt, and C. P. Mathews, "Closed-form 2-D angle estimation with rectangular arrays in element space or beamspace via unitary ESPRIT," *IEEE Trans. Signal Process.*, vol. 44, no. 2, pp. 316-328, Feb. 1996.
- [8] R. O. Schmidt, "Multiple emitter location and signal parameter estimation," *IEEE Trans. Antennas Propag.*, vol. 34, no. 3, pp. 276-280, Mar. 1986.

- [9] A. Swindlehurst and T. Kailath, "A performance analysis of sub space-based methods in the presence of model errors. I. The MUSIC algorithm," *IEEE Trans. Signal Process.*, vol. 40, no. 7, pp. 1578-1774, Jul. 1992.
- [10] I. Ziskind and M. Wax, "Maximum likelihood localization of multiple sources by alternating projection," *IEEE Trans. Acust., Speech, Signal Process.*, vol. 36, no. 10, pp. 1553-1560, Oct. 1988.
- [11] P. Stoica and A. B. Gershman, "Maximum-likelihood DOA estimation by data-supported grid search," *IEEE Signal Process. Lett.*, vol. 6, no. 10, pp. 273-275, Oct. 1999.
- [12] A. H. El Zooghby, C. G. Christodoulou, and M. Georgiopoulos, "Performance of radial-basis function networks for direction of arrival estimation with antenna arrays," *IEEE Trans. Antennas Propag.*, vol. 45, no. 11, pp. 1611-1617, Nov. 1997.
- [13] A. H. El Zooghby, C. G. Christodoulou, and M. Georgiopoulos, "A neural network-based smart antenna for multiple source tracking," *IEEE Trans. Antennas Propag.*, vol. 48, pp. 768-776, May 2000.
- [14] M. Martinez-Ramon and C. G. Christodoulou, *Support Vector Machines for Antenna Array Processing and Electromagnetics*. Synthesis Lectures on Computational Electromagnetics Lecture #5, Morgan & Claypool Publishers, 2006.
- [15] V. Vapnik, *Statistical Learning Theory*. New York: Wiley, 1998.
- [16] E. Bermani, A. Boni, S. Caorsi, M. Donelli, and A. Massa, "A multi-source strategy based on a learning-by-examples technique for buried object detection," *Progress In Electromagnetic Research, PIER*, vol. 48, pp. 185-200, 2004.
- [17] A. Massa, A. Boni, and M. Donelli, "A classification approach based on SVM for electromagnetic subsurface sensing," *IEEE Trans. Geosci. Remote Sens.*, vol. 43, no. 9, pp. 2084-2093, Sep. 2005.

- [18] D. Anguita, A. Boni, and S. Ridella, "A digital architecture for support vector machines: theory, algorithm and FPGA implementation," *IEEE Trans. Neural Netw.*, vol. 14, no. 5, pp. 993-1009, Sep. 2003.
- [19] M. Pastorino and A. Randazzo, "A smart antenna system for direction of arrival estimation based on a support vector regression," *IEEE Trans. Antennas Propag.*, vol. 53, no. 7, pp. 2161-2168, Jul. 2005.
- [20] M. Pastorino and A. Randazzo, "The SVM-based smart antenna for estimation of the directions of arrival of electromagnetic waves," *IEEE Trans. Instrum. Meas.*, vol. 55, no. 6, pp. 1918-1925, Dec. 2006.
- [21] A. Randazzo, M. A. Abou-Khousa, M. Pastorino, and R. Zoughi, "Direction of arrival estimation based on support vector regression: experimental validation and comparison with MUSIC," *IEEE Trans. Antennas Wireless Propag. Lett.*, vol. 6, pp. 379-382, 2007.
- [22] S. Caorsi, M. Donelli, D. Franceschini, and A. Massa, "A new methodology based on an iterative multiscaling for microwave imaging," *IEEE Trans. Microw. Theory Tech.*, vol. 51, no. 4, pp. 1162-1173, Apr. 2003.
- [23] L. C. Godara, "Applications of antenna arrays to mobile communications - Part I: Performance improvement, feasibility, and system considerations," *Proc. IEEE*, vol. 85, pp. 1031-1060, Jul. 1997.
- [24] C.A. Balanis, *Antenna theory: Analysis and design*. New York: Wiley, 2005.
- [25] A. Manikas, A. Alexiou, H. R. Karimi, "Comparison of the ultimate direction-finding capabilities of a number of planar array geometries," *IEE Proc. Radar, Sonar Navig.*, vol. 144, no. 6, pp. 321-329, Dec. 1997.
- [26] C. G. Christodoulou and M. Georgiopoulos, *Applications of Neural Networks in Electromagnetics*. Artech House Inc., Boston, MA, USA, 2001.
- [27] W. Chen, J. Jen, and S. M. Zhang, "Planar dipole arrays with equal element input impedances," *Electron. Lett.*, vol. 31, no. 24, pp. 2061-2062, 1995.

FIGURE CAPTIONS

- **Figure 1.** Planar array geometry.
- **Figure 2.** *IMSA – DOA Procedure* - Angular region partitioning and *ARoIs* identification at the steps $s = 1$ (a) and $s = 2$ (b).
- **Figure 3.** *Single signal scenario*, $I = 1$ - Probability map determined by the *IMSA – DOA* procedure at: (a) $s = 2$, (b) $s = S_{opt} = 4$.
- **Figure 4.** *Single signal scenario*, $I = 1$ - Probability maps obtained with different classification approaches: (a) single-step *SVM*, (b) multi layer perceptron (*MLP*) neural network, and (c) radial basis function (*RBF*) neural network [$\Delta\theta = 1.25^\circ$ and $\Delta\phi = 5^\circ$].
- **Figure 5.** *Single signal scenario*, $I = 1$ - Uniform (red points) and non-uniform (green triangles) angular training sets.
- **Figure 6.** *Single signal scenario*, $I = 1$ - Behavior of the location index versus the number of failed array elements.
- **Figure 7.** *Multiple signals scenario*, $I = 2$ - Probability maps obtained with different classification approaches: *IMSA – SVM* [(a) $s = 1$, (b) $s = 2$, (c) $s = S_{opt} = 3$], (d) single-step *SVM*, (e) multi layer perceptron (*MLP*) neural network, and (f) radial basis function (*RBF*) neural network [$\Delta\theta = \Delta\theta_{(2)}^{(3)} = 2.5^\circ$ and $\Delta\phi = \Delta\phi_{(2)}^{(3)} = 10^\circ$].
- **Figure 8.** *Multiple signals scenario*, $I = 3$ (*Configuration 1/1/1*) - Probability maps obtained with different classification approaches: (a) *IMSA – SVM* [$s = S_{opt} = 3$] and (b) single-step *SVM* [$\Delta\theta = \Delta\theta_{(2)}^{(3)}$ and $\Delta\phi = \Delta\phi_{(2)}^{(3)}$].
- **Figure 9.** *Multiple signals scenario*, $I = 4$ - Probability maps obtained with the *IMSA – SVM*. *Configuration 1/1/1/1*: step (a) $s = 1$, (b) $s = 2$, and (c) $s = S_{opt} = 3$; *Configuration 2/2*: step $s = S_{opt} = 3$ (d); *Configuration 1/3*: step $s = S_{opt} = 3$ (e).
- **Figure 10.** *Multiple signals scenario* ($I = 18$ - *Clustered Distribution*) - Probability maps obtained with different classification approaches: (a) *IMSA – SVM* ($s = S_{opt} = 3$), (b)

single-step *SVM*, (c) multi layer perceptron (*MLP*) neural network, and (d) radial basis function (*RBF*) neural network [$\Delta\theta = \Delta\theta_{(2)}^{(3)}$ and $\Delta\phi = \Delta\phi_{(2)}^{(3)}$].

- **Figure 11.** *Multiple signals scenario* ($I = 18$ - *Sparse Distribution*) - Probability maps determined by the *IMSA – SVM* at the convergence ($s = S_{opt} = 2$ - $\Delta\theta_{(1)}^{(2)} = 5^\circ$ and $\Delta\phi_{(1)}^{(2)} = 20^\circ$).
- **Figure 12.** *No-signals scenario* [$I = 0$; $P_n = 20$ dB (*Test Set*) - $P_n = 0$ dB (*Training Set*)] - Probability maps obtained with different classification approaches: (a) *IMSA – SVM* ($s = S_{opt} = 1$), (b) multi layer perceptron (*MLP*) neural network, and (c) radial basis function (*RBF*) neural network.
- **Figure 13.** *Dipole Array*, $I = 1$ - Probability map determined by the *IMSA – DOA* [$s = S_{opt} = 4$].
- **Figure 14.** *Dipole Array*, $I = 2$ - Probability map determined by the *IMSA – DOA* when (a) $I_1 = (\theta_1 = 12^\circ, \phi_1 = 165^\circ)$, $I_2 = (\theta_2 = 82^\circ, \phi_2 = 165^\circ)$ [$s = S_{opt} = 3$] and (b) $I_1 = (\theta_1 = 30^\circ, \phi_1 = 60^\circ)$, $I_2 = (\theta_2 = 30^\circ, \phi_2 = 300^\circ)$ [$s = S_{opt} = 3$].

TABLE CAPTIONS

- **Tab. I.** Statistics of the averaged performance indexes ($\hat{\zeta} = \sum_{i=1}^I \zeta^{(i)}$ and $\hat{\psi} = \sum_{i=1}^I \psi^{(i)}$) for different signal configurations ($I = 1, 2, 3, 4$).
- **Table II.** *Single signal scenario*, $I = 1$ - *Comparative assessment*. Values of the location index ζ when applying *IMSA – DOA*, *SVR*, *MUSIC*, and *ESPRIT*.
- **Table III.** *Multiple signals scenario*, $I = 2$. Performance indexes when applying *IMSA – DOA*, single-step *SVM*, multi layer perceptron (*MLP*) neural network, and radial basis function (*RBF*) neural network.
- **Table IV.** *Multiple signals scenario*, $I = 3$ (*Configuration 1/1/1*). Performance indexes when applying *IMSA – DOA*, single-step *SVM*, multi layer perceptron (*MLP*) neural network, and radial basis function (*RBF*) neural network.

- **Table V.** *Multiple signals scenario, $I = 4$ (Configuration 1/1/1/1).* Performance indexes when applying *IMSA – DOA*, single-step *SVM*, multi layer perceptron (*MLP*) neural network, and radial basis function (*RBF*) neural network.
- **Table VI** *Multiple signals scenario, $I = 4$ (Configuration 2/2).* Performance indexes when applying *IMSA – DOA*, single-step *SVM*, multi layer perceptron (*MLP*) neural network, and radial basis function (*RBF*) neural network.
- **Table VII.** *Multiple signals scenario, $I = 4$ (Configuration 1/3).* Performance indexes when applying *IMSA – DOA*, single-step *SVM*, multi layer perceptron (*MLP*) neural network, and radial basis function (*RBF*) neural network.
- **Table VIII.** *Multiple signals scenario, $I = 18$ (Clustered Distribution).* Performance indexes when applying *IMSA – DOA*, single-step *SVM*, multi layer perceptron (*MLP*) neural network, and radial basis function (*RBF*) neural network.

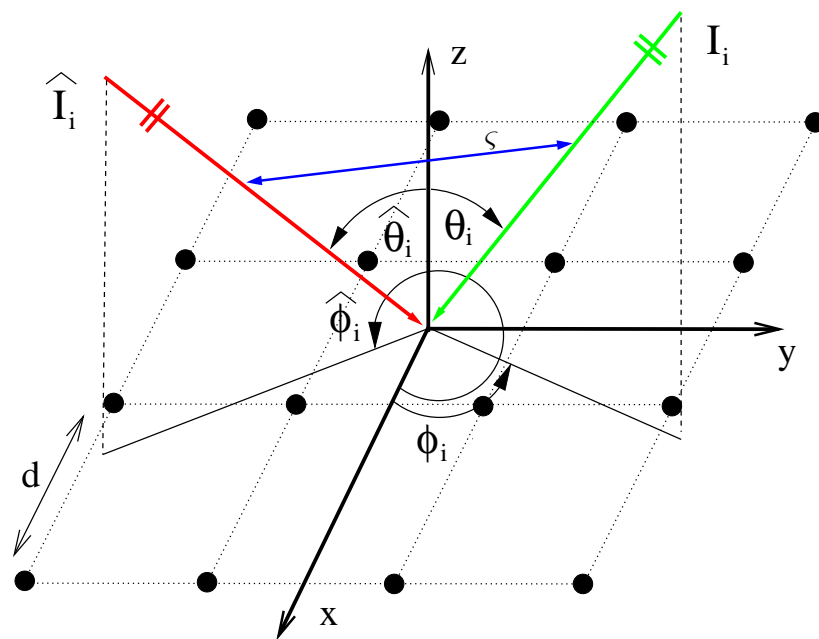
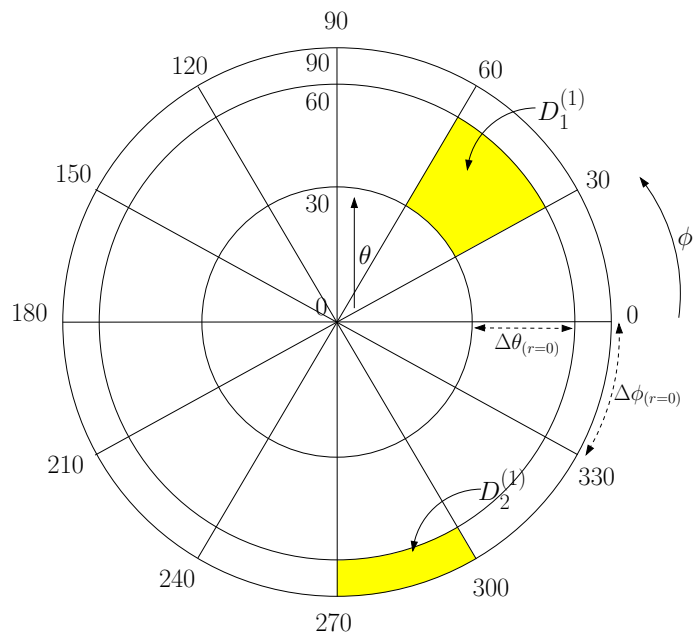
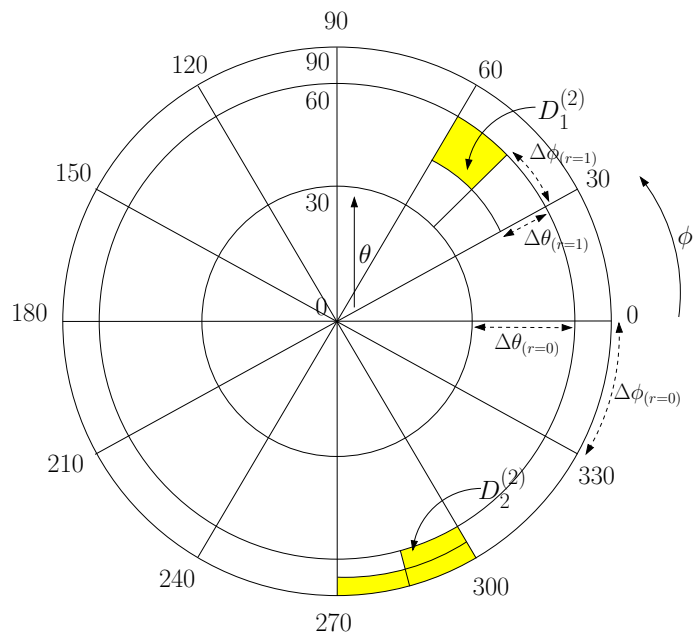


Fig. 1 - M. Donelli *et al.*, "An Innovative Multi-Resolution Approach..."

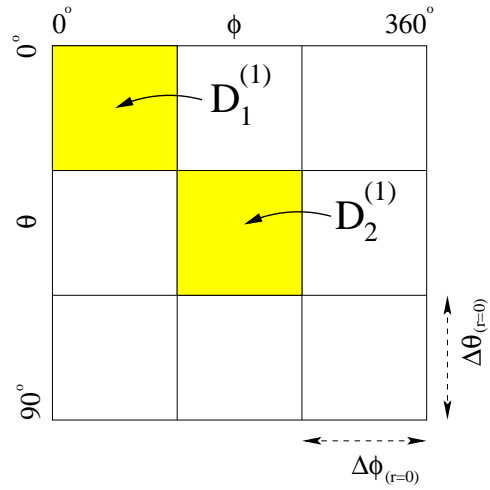


(a)

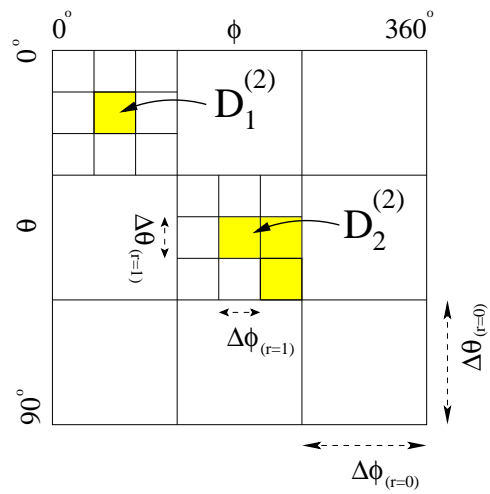


(b)

Fig. 2 - M. Donelli *et al.*, "An Innovative Multi-Resolution Approach..."

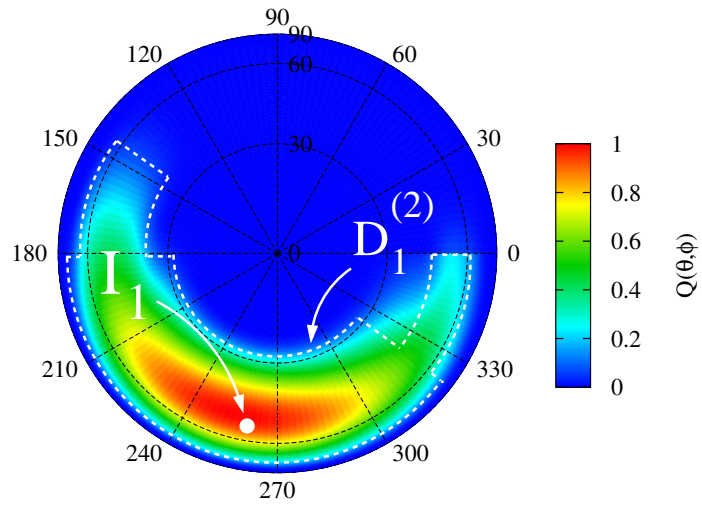


(a)

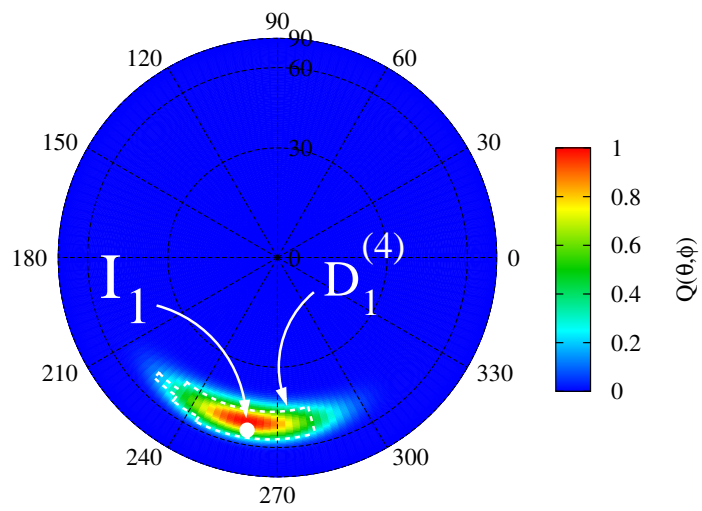


(b)

Fig. 2 - M. Donelli *et al.*, “An Innovative Multi-Resolution Approach...”

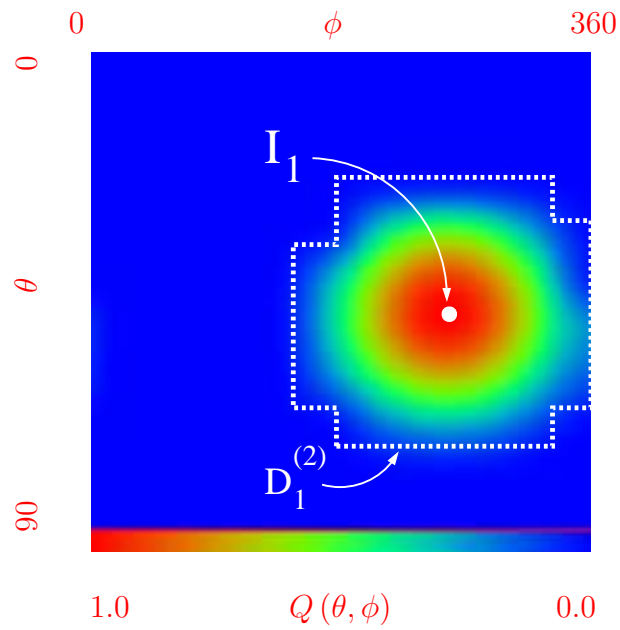


(a)

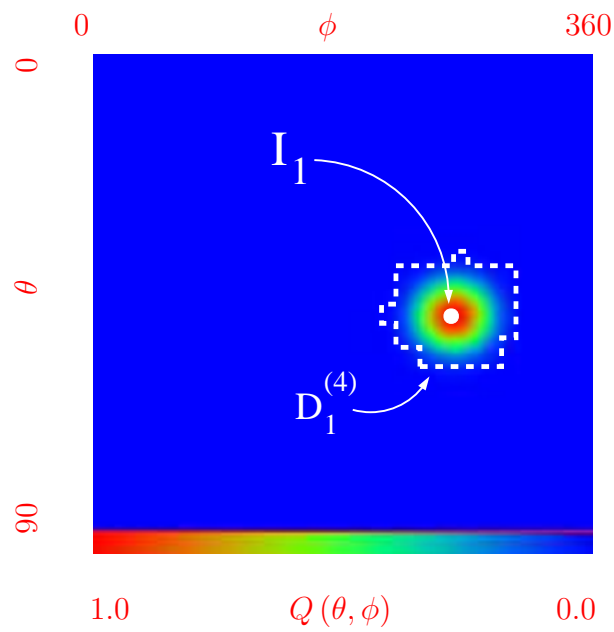


(b)

Fig. 3 - M. Donelli *et al.*, "An Innovative Multi-Resolution Approach..."

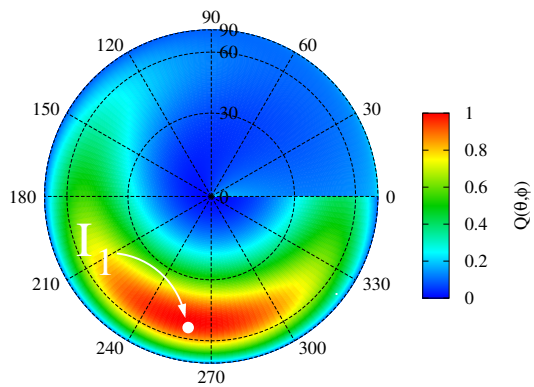


(a)

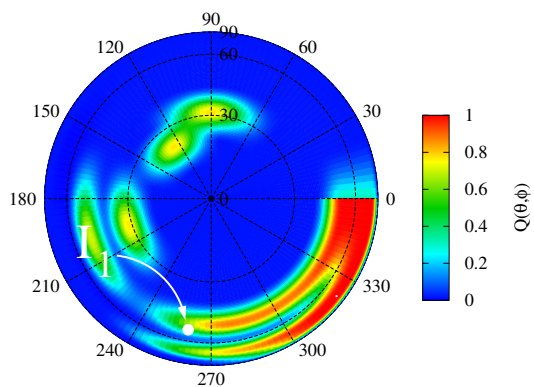


(b)

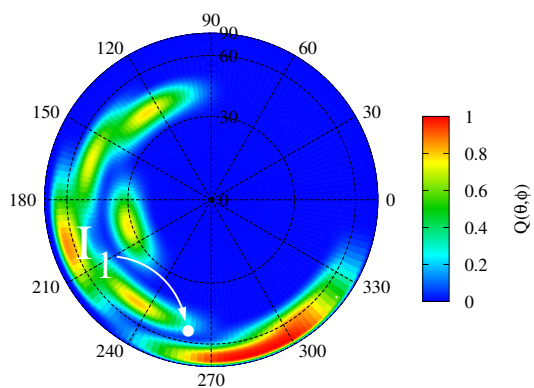
Fig. 3 - M. Donelli *et al.*, "An Innovative Multi-Resolution Approach..."



(a)



(b)



(c)

Fig. 4 - M. Donelli *et al.*, "An Innovative Multi-Resolution Approach..."

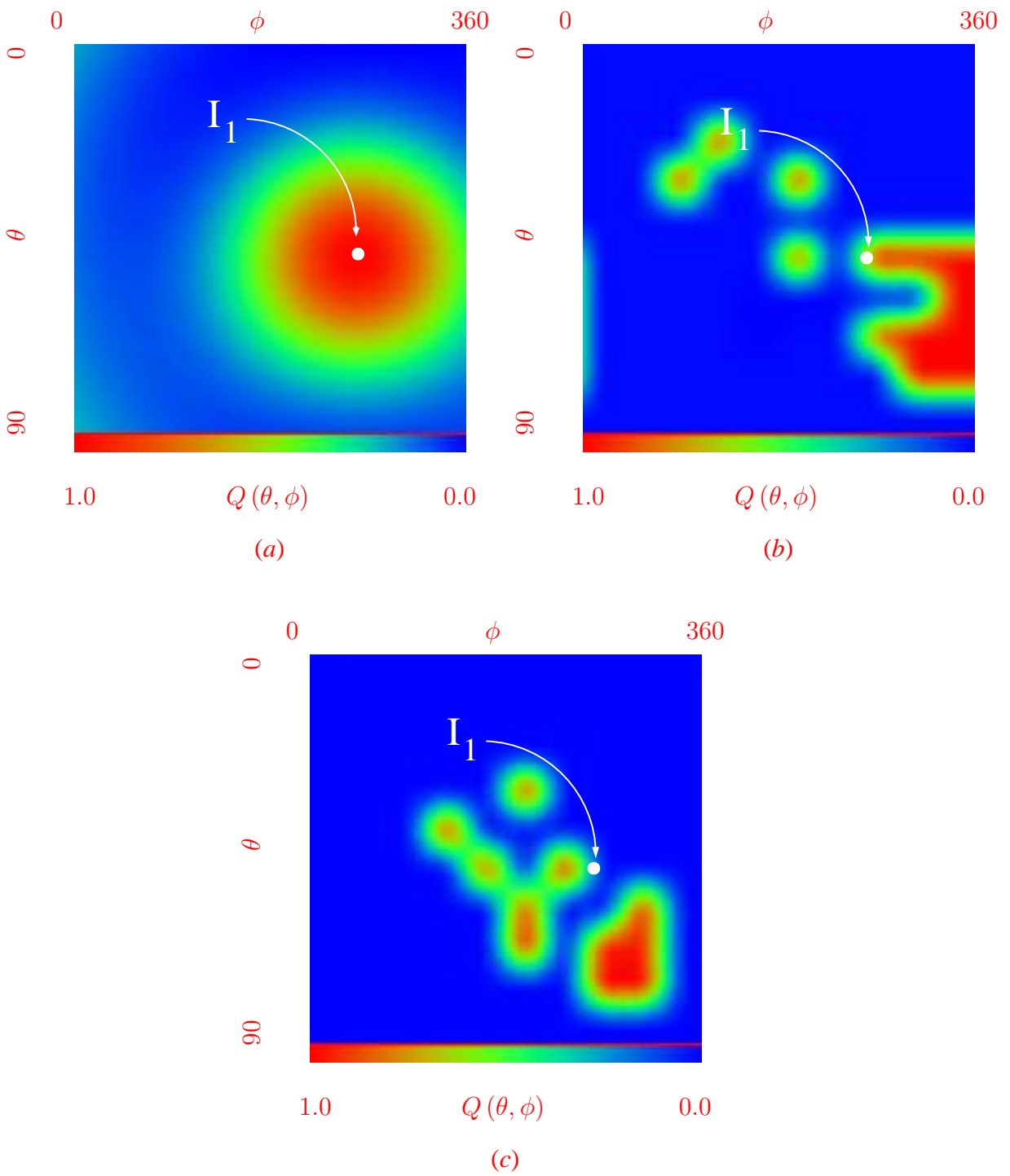


Fig. 4 - M. Donelli *et al.*, "An Innovative Multi-Resolution Approach..."

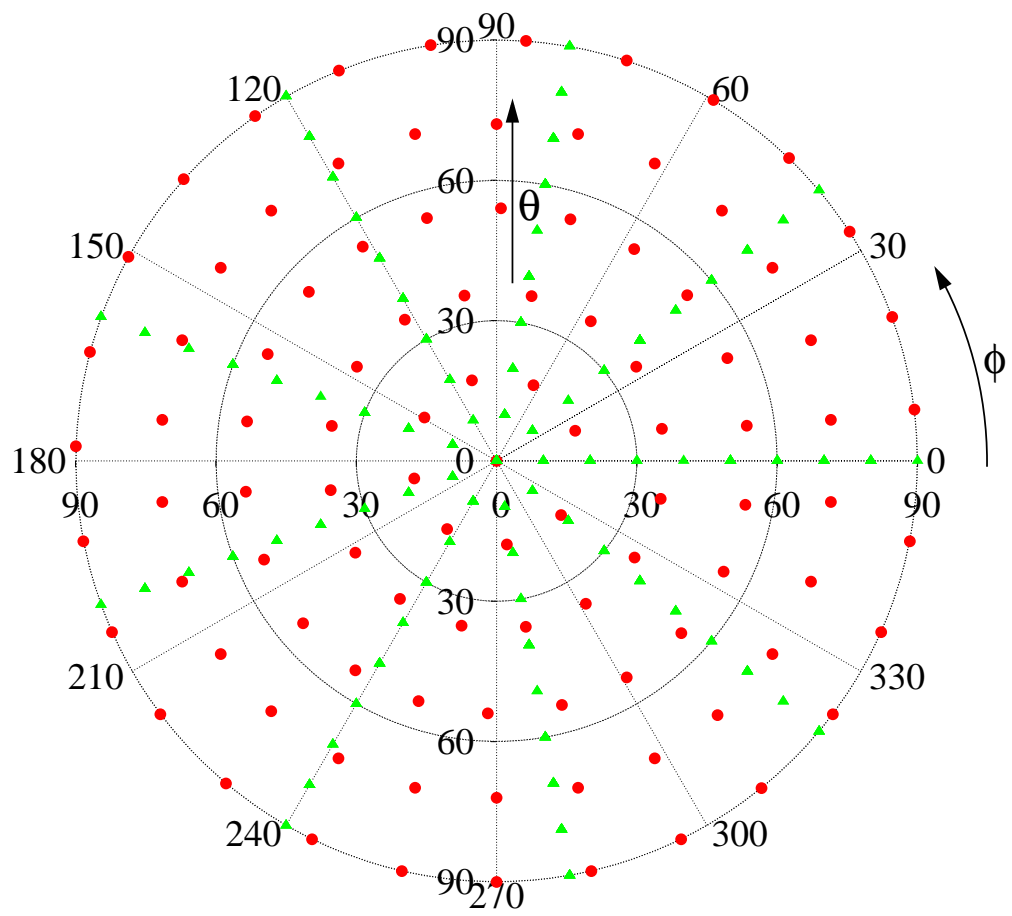


Fig. 5 - M. Donelli *et al.*, “An Innovative Multi-Resolution Approach...”

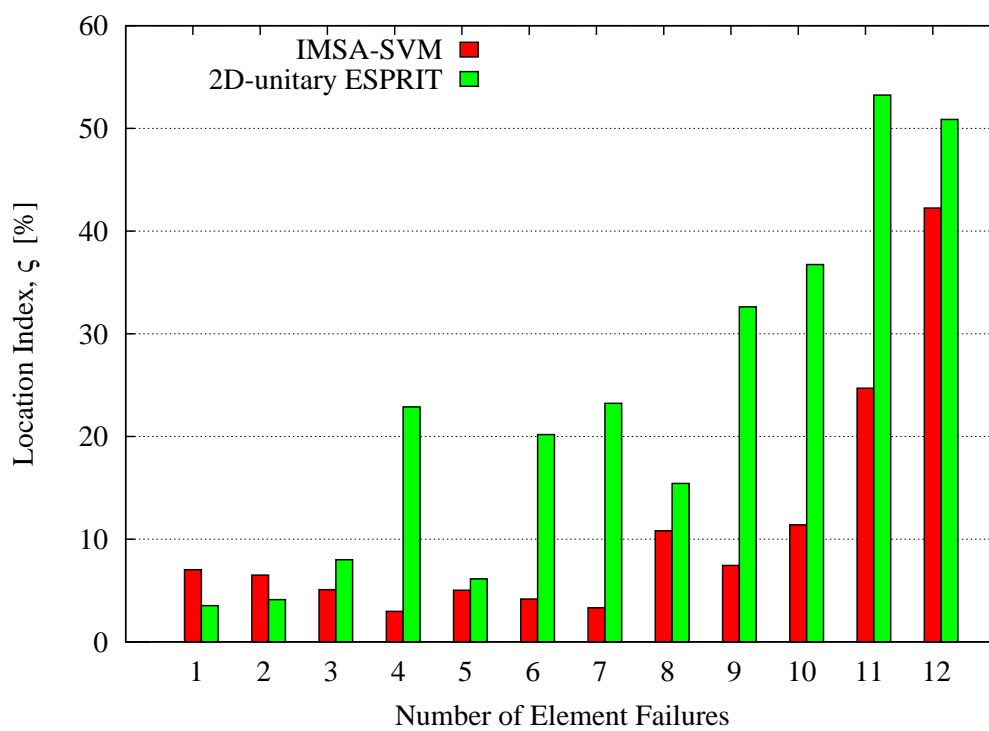
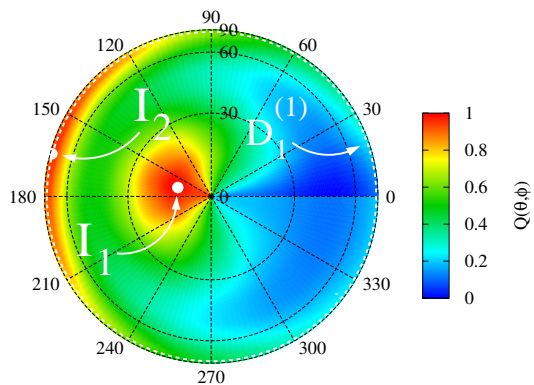
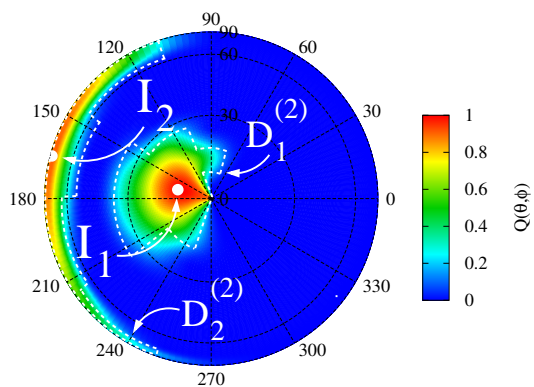


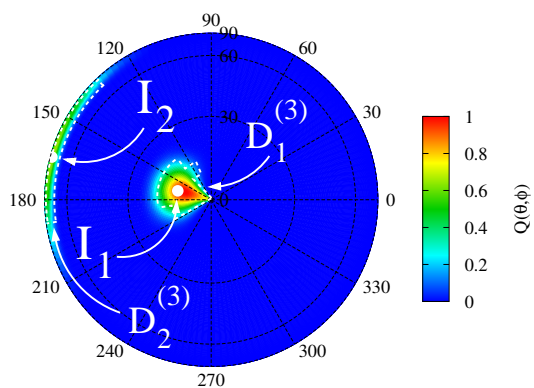
Fig. 6 - M. Donelli *et al.*, “An Innovative Multi-Resolution Approach...”



(a)



(b)



(c)

Fig. 7(I) - M. Donelli *et al.*, "An Innovative Multi-Resolution Approach..."

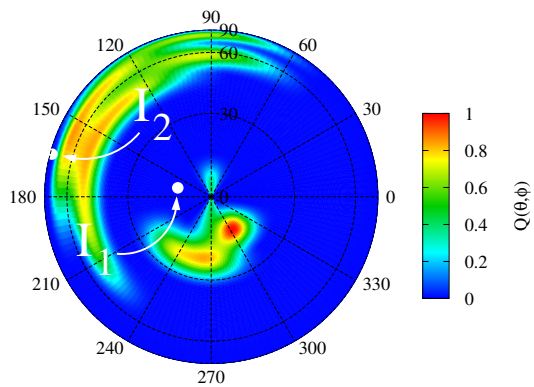
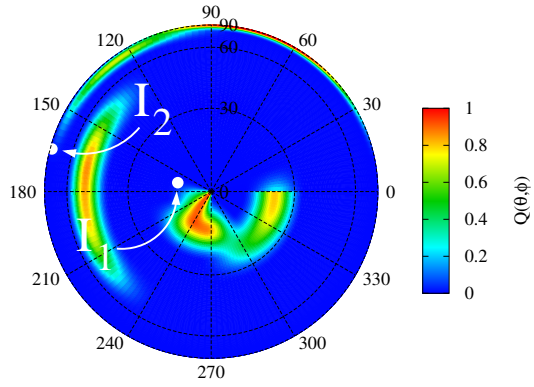
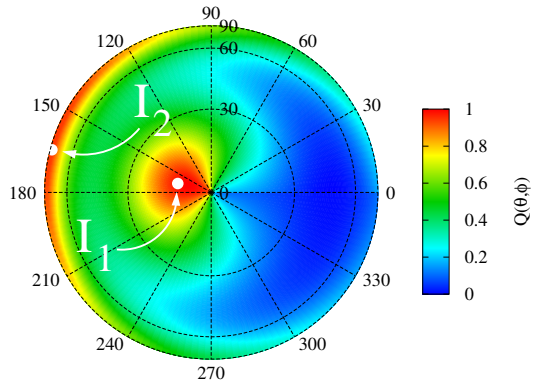


Fig. 7(II) - M. Donelli *et al.*, "An Innovative Multi-Resolution Approach..."

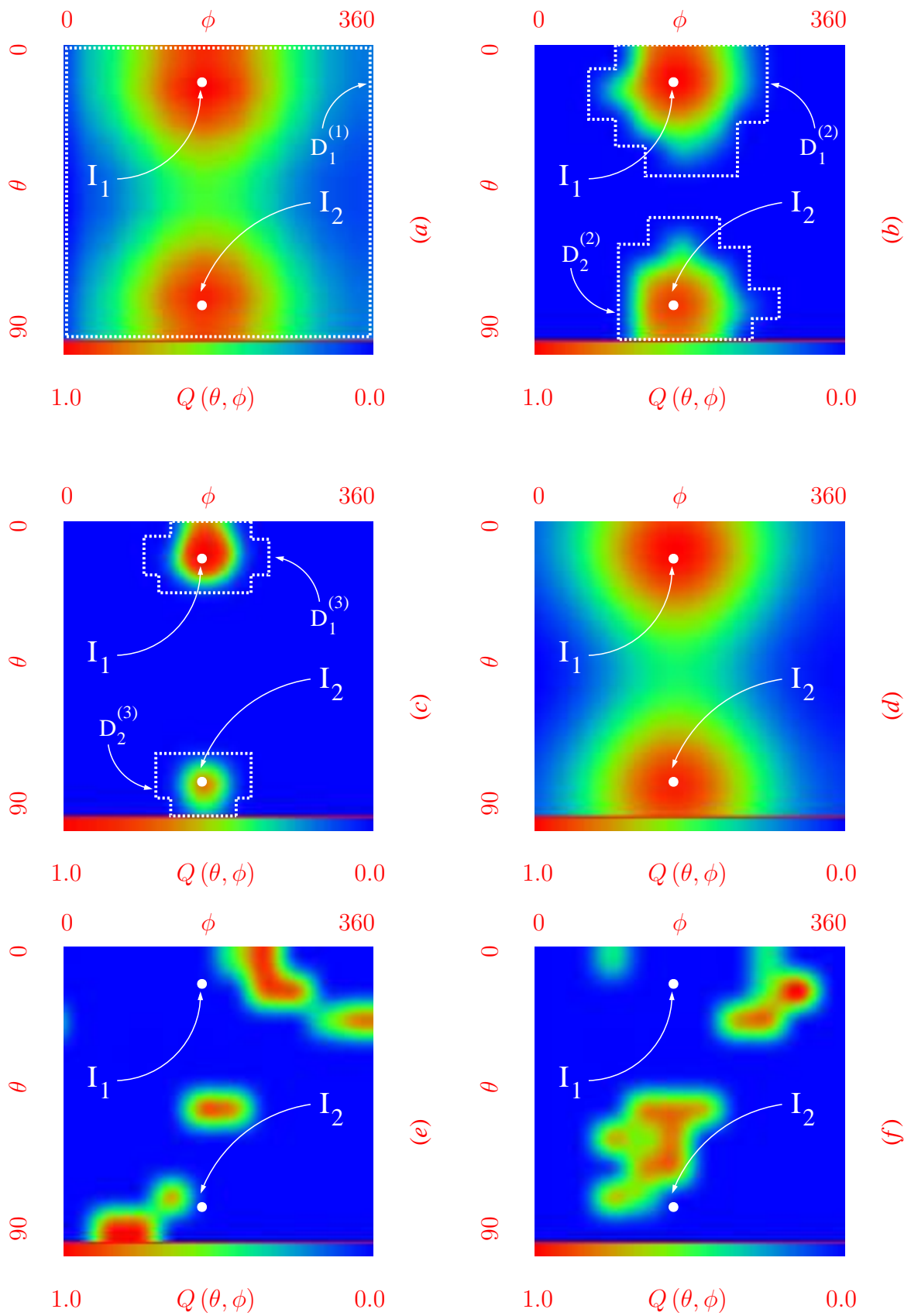
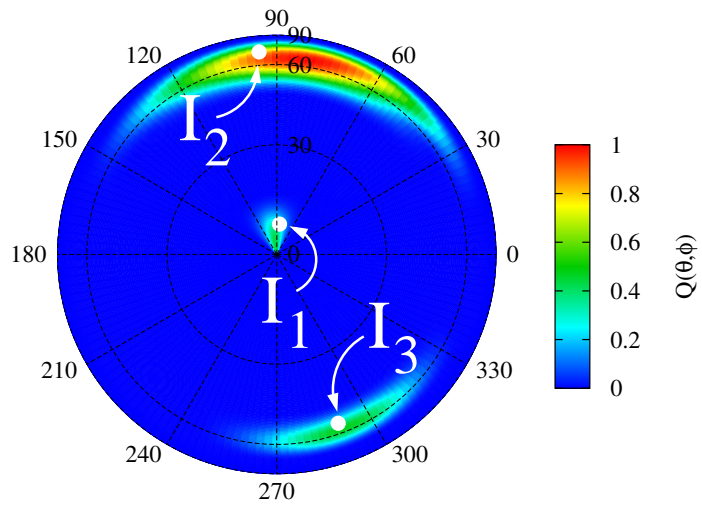
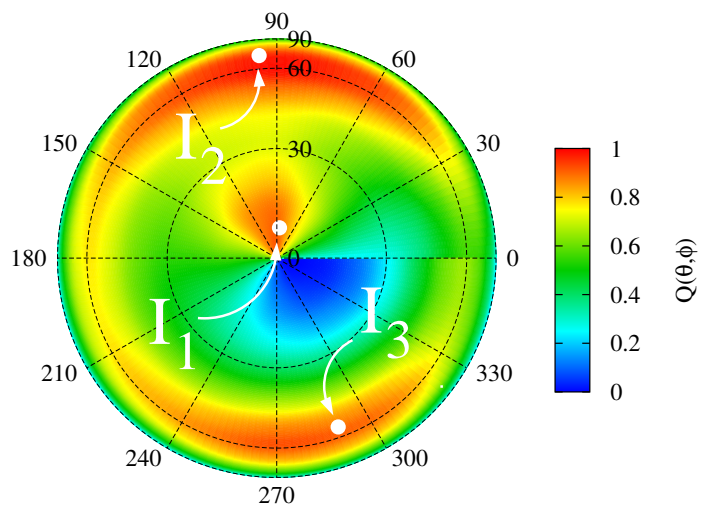


Fig. 7 - M. Donelli *et al.*, "An Innovative Multi-Resolution Approach..."

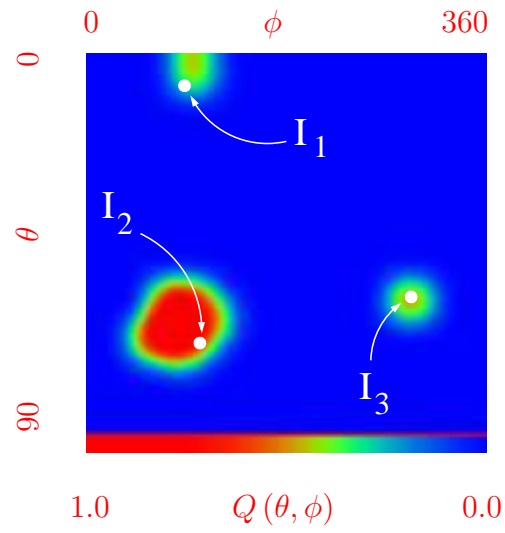


(a)

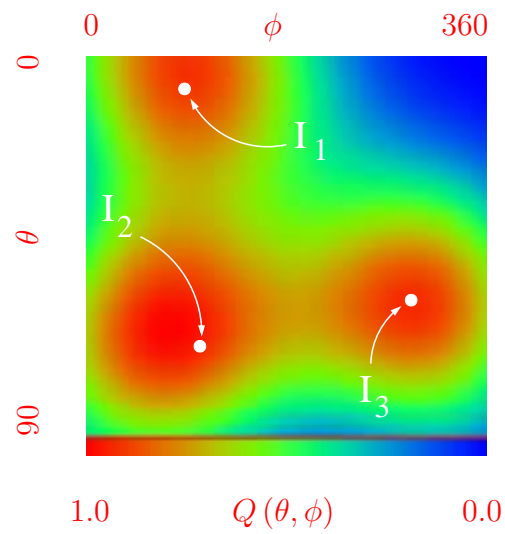


(b)

Fig. 8 - M. Donelli *et al.*, "An Innovative Multi-Resolution Approach..."

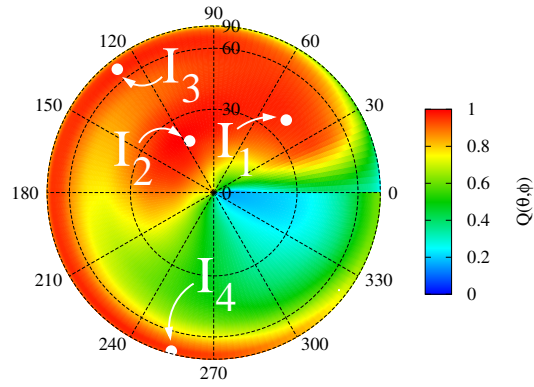


(a)

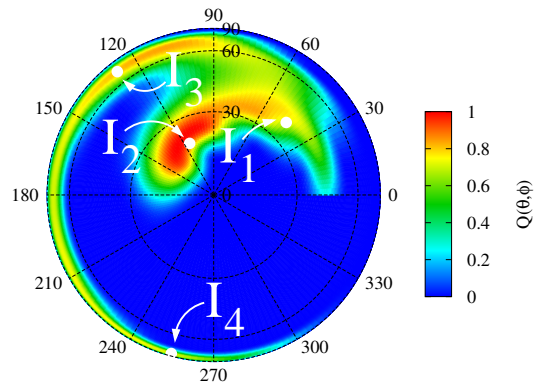


(b)

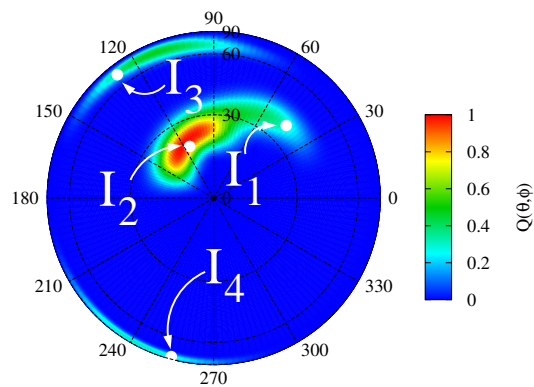
Fig. 8 - M. Donelli *et al.*, "An Innovative Multi-Resolution Approach..."



(a)

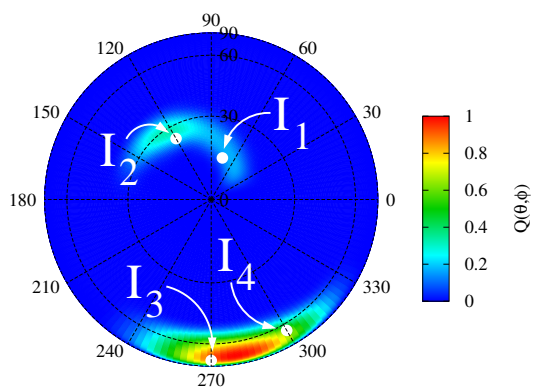


(b)

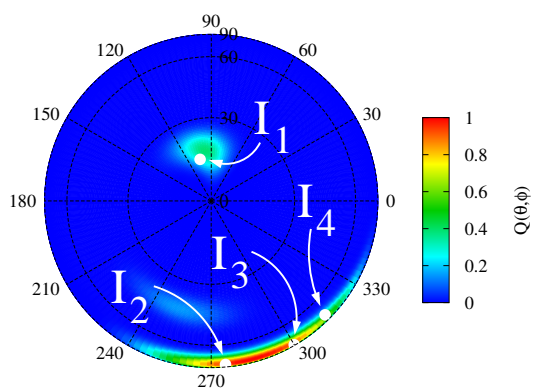


(c)

Fig. 9(I) - M. Donelli *et al.*, "An Innovative Multi-Resolution Approach..."



(d)



(e)

Fig. 9(II) - M. Donelli *et al.*, "An Innovative Multi-Resolution Approach..."

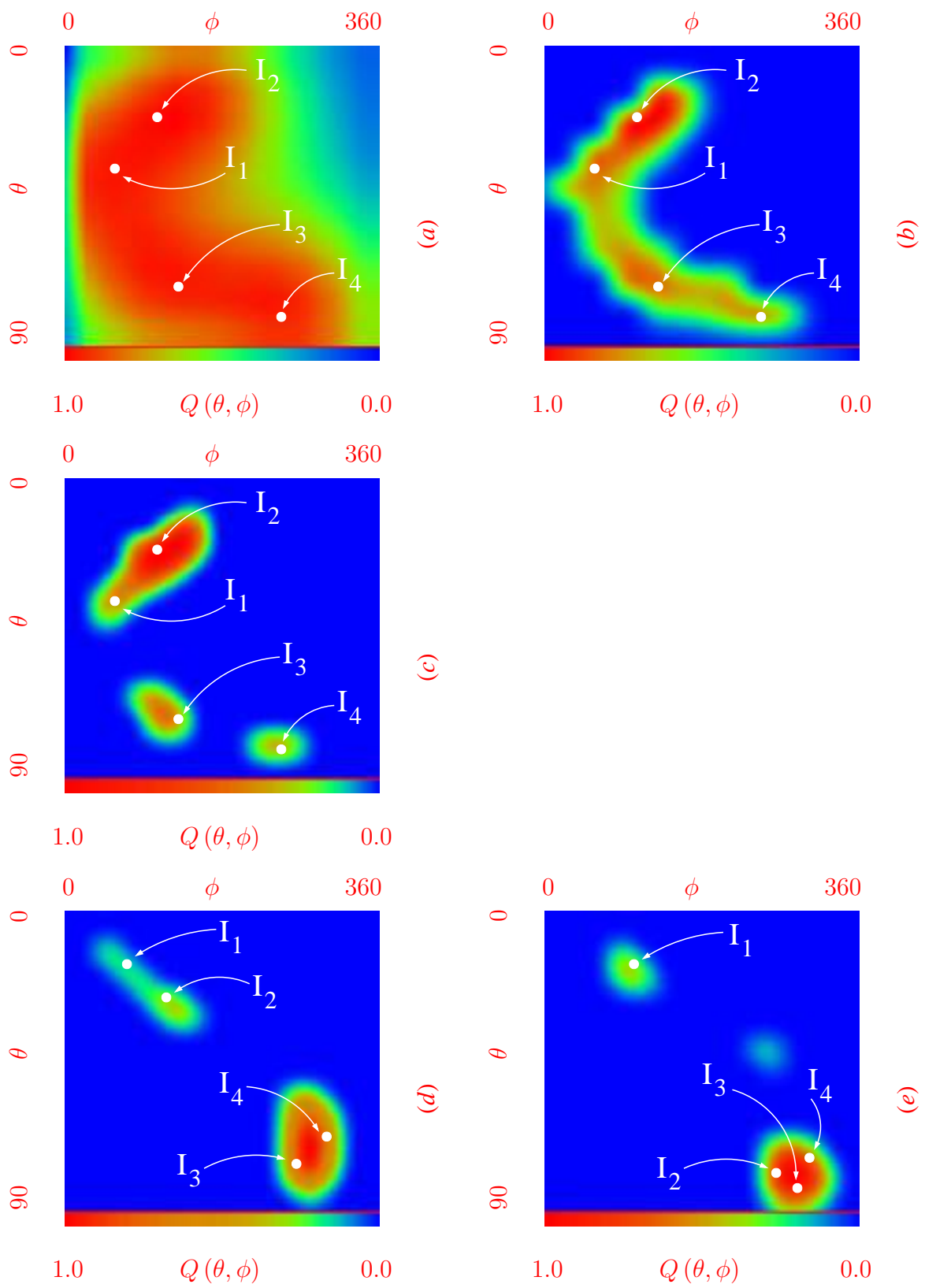
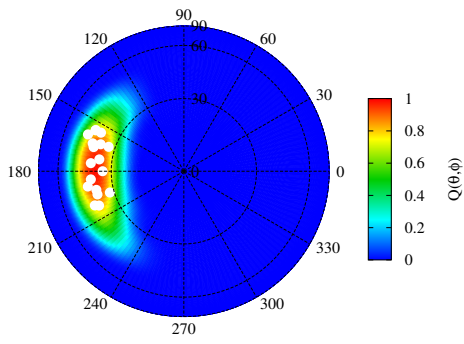
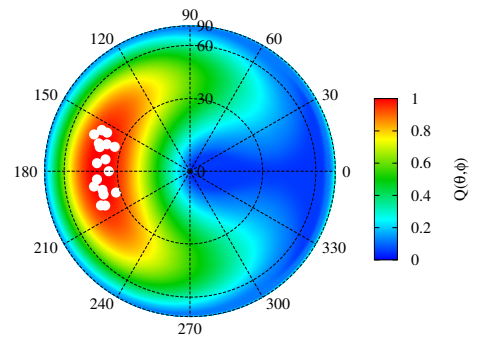


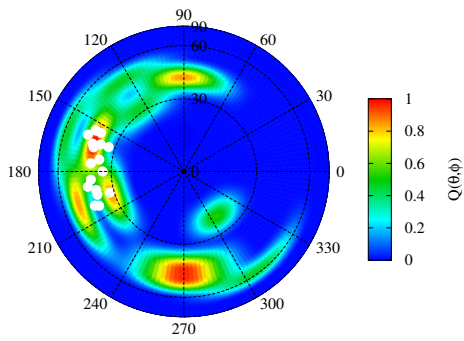
Fig. 9 - M. Donelli *et al.*, "An Innovative Multi-Resolution Approach..."



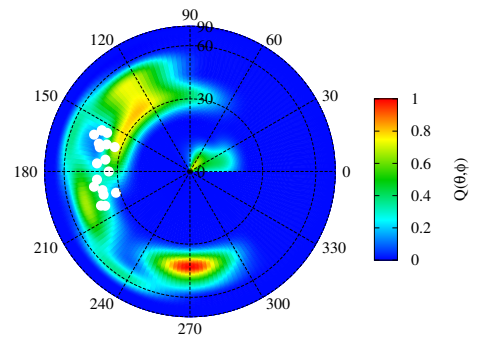
(a)



(b)



(c)



(d)

Fig. 10 - M. Donelli *et al.*, "An Innovative Multi-Resolution Approach..."

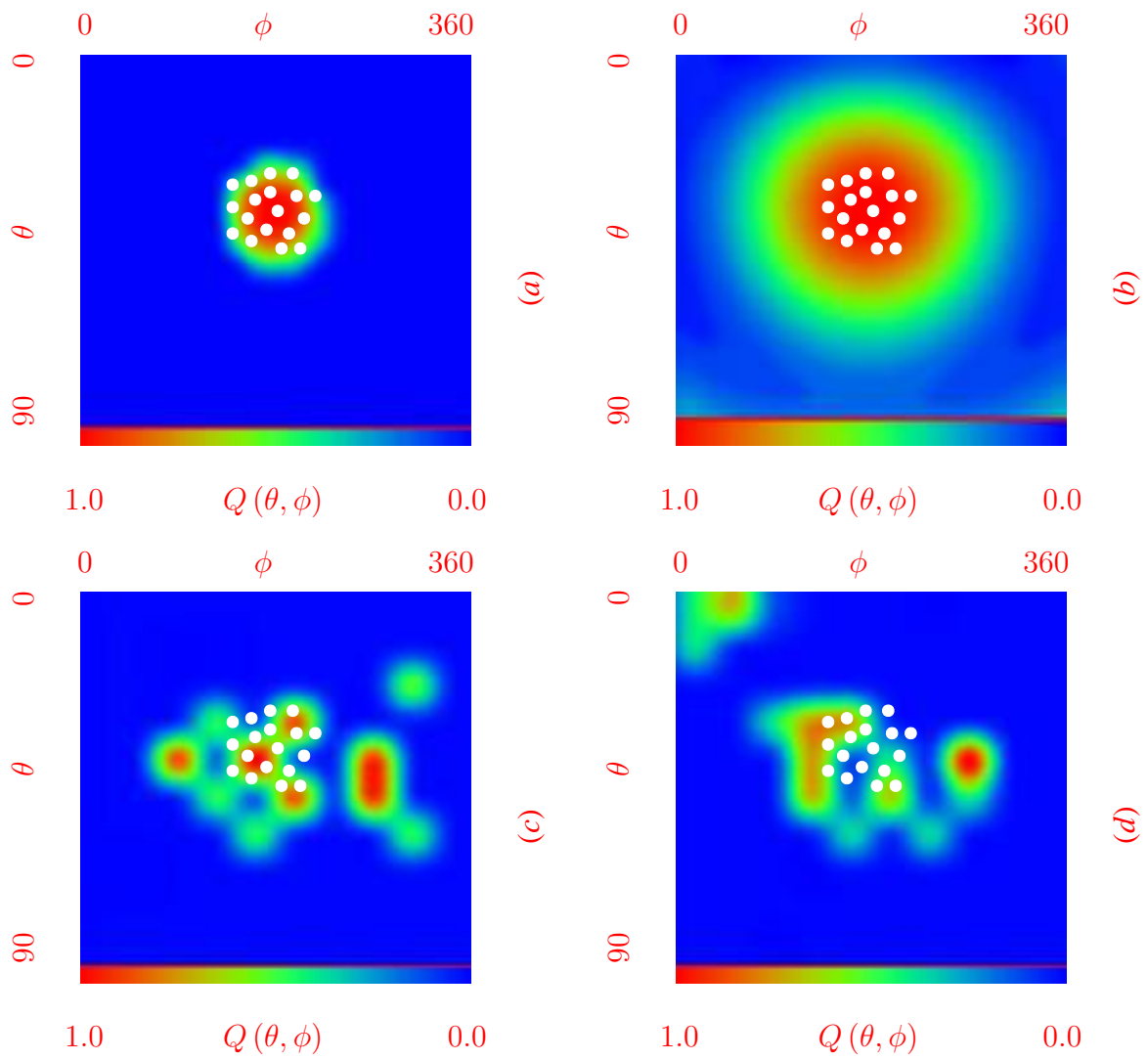


Fig. 10 - M. Donelli *et al.*, "An Innovative Multi-Resolution Approach..."

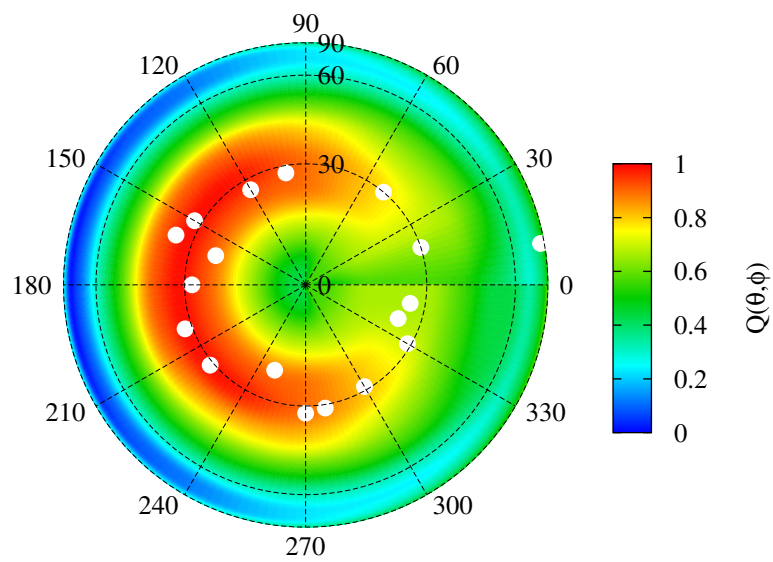


Fig. 11 - M. Donelli *et al.*, "An Innovative Multi-Resolution Approach..."

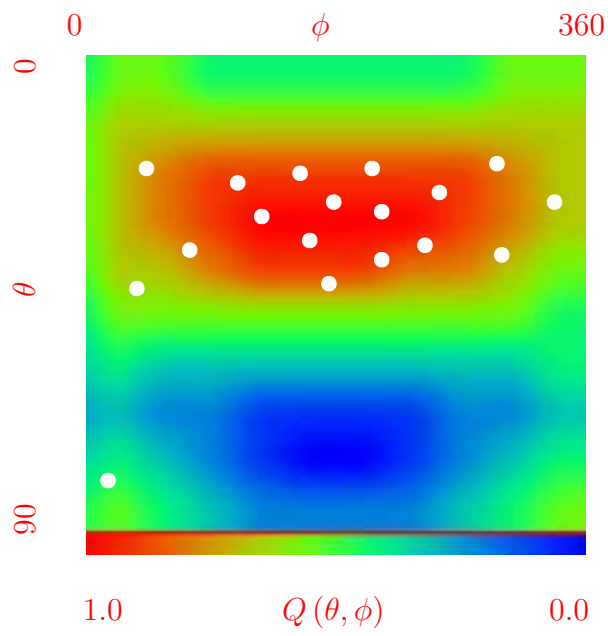
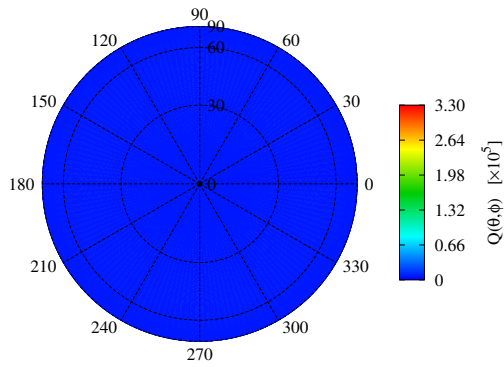
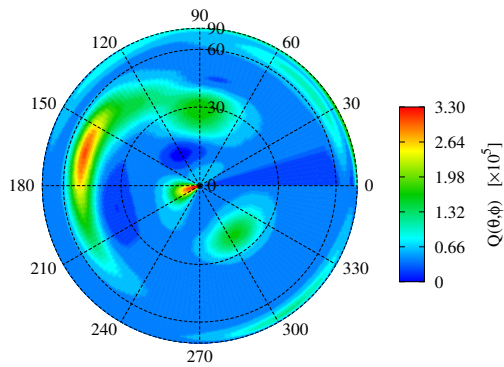


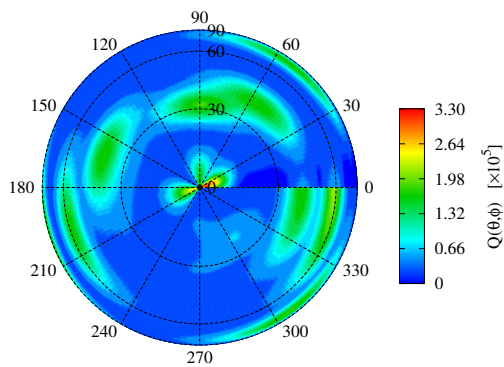
Fig. 11 - M. Donelli *et al.*, "An Innovative Multi-Resolution Approach..."



(a)



(b)



(c)

Fig. 12 - M. Donelli *et al.*, "An Innovative Multi-Resolution Approach..."

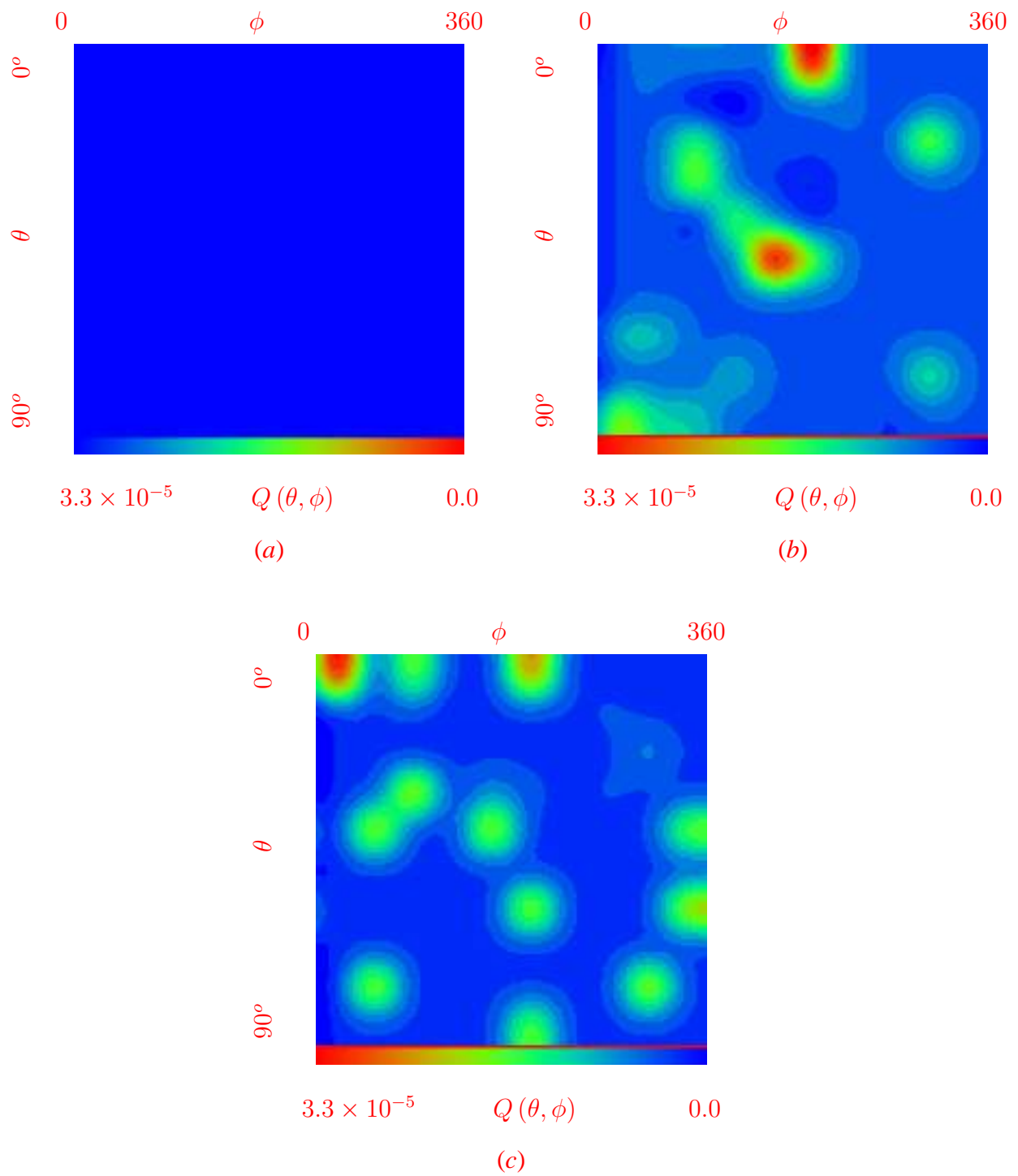


Fig. 12 - M. Donelli *et al.*, "An Innovative Multi-Resolution Approach..."

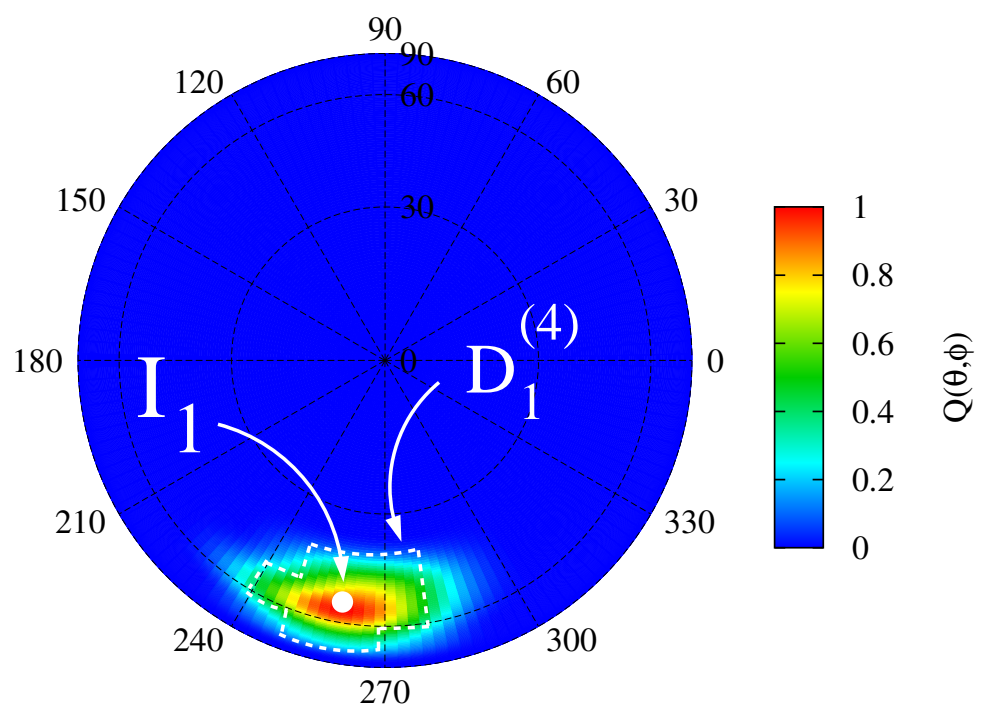


Fig. 13 - M. Donelli *et al.*, "An Innovative Multi-Resolution Approach..."

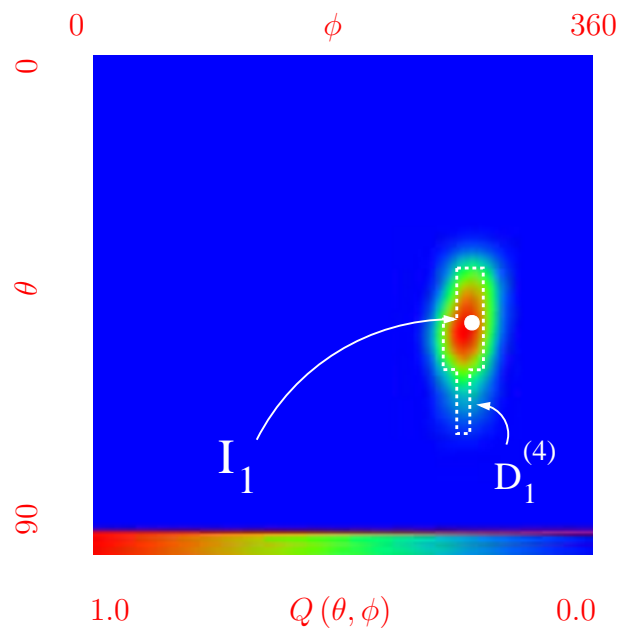
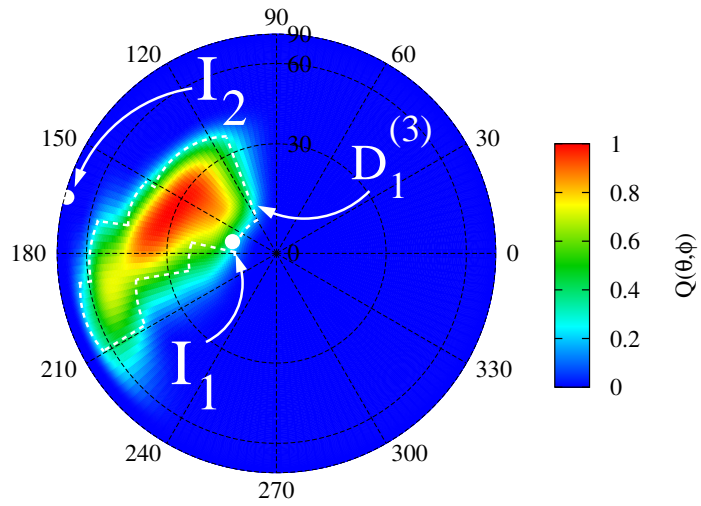
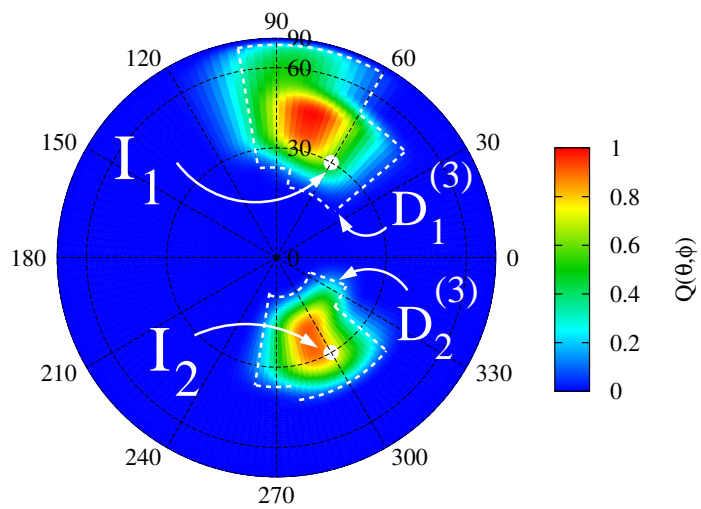


Fig. 13 - M. Donelli *et al.*, "An Innovative Multi-Resolution Approach..."

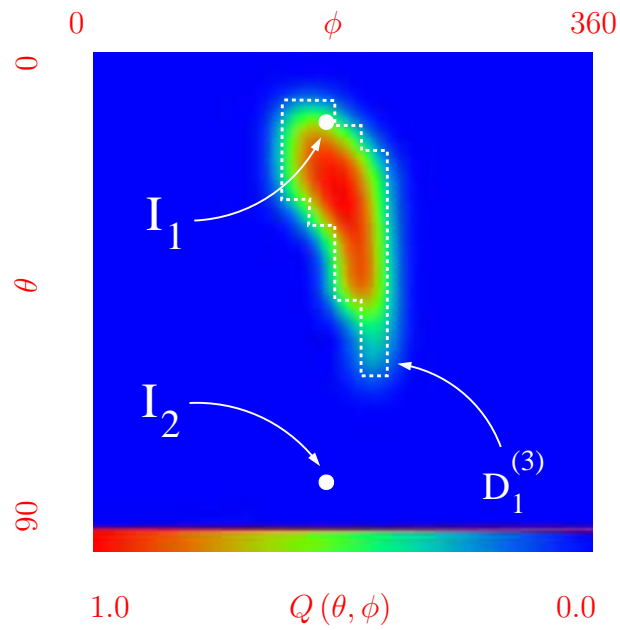


(a)

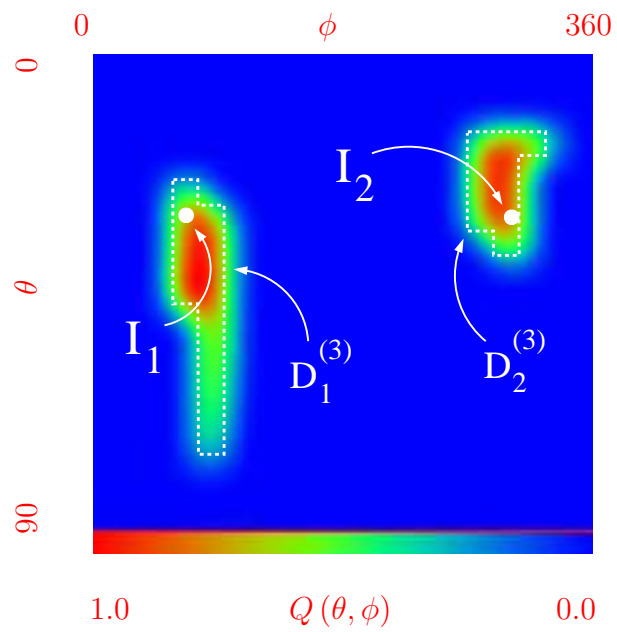


(b)

Fig. 14 - M. Donelli *et al.*, "An Innovative Multi-Resolution Approach..."



(a)



(b)

Fig. 14 - M. Donelli *et al.*, "An Innovative Multi-Resolution Approach..."

	<i>Min</i>	<i>Max</i>	<i>Avg</i>	<i>Var</i>
<i>Single Signal (I = 1)</i>				
$\hat{\zeta}$	0.16	43.25	2.81	8.76
$\hat{\psi}$	0.02	9.14	0.25	1.35
<i>Multiple Signals (I = 2)</i>				
$\hat{\zeta}$	0.31	58.47	4.51	8.56
$\hat{\psi}$	0.007	11.05	0.28	1.54
<i>Multiple Signals (I = 3)</i>				
$\hat{\zeta}$	0.38	17.35	5.55	2.14
$\hat{\psi}$	0.009	0.37	0.15	0.34
<i>Multiple Signals (I = 4)</i>				
$\hat{\zeta}$	0.47	70.72	17.29	13.58
$\hat{\psi}$	0.005	1.89	0.17	0.69

Tab. I - M. Donelli *et al.*, “An Innovative Multi-Resolution Approach...”

	<i>DOA Method</i>					
θ_1	<i>ESPRIT</i>	<i>2D ESPRIT</i>	<i>MUSIC</i>	<i>SVR</i>	<i>IMSA – SVM^(unif)</i>	<i>IMSA – SVM</i>
20°	0.16	0.08	0.34	1.21	0.75	0.52
40°	0.51	0.22	0.59	1.38	1.17	0.83
60°	0.51	0.27	0.68	1.64	1.52	2.22
80°	0.68	0.36	0.74	1.56	1.64	4.93

Tab. II - M. Donelli *et al.*, “An Innovative Multi-Resolution Approach...”

<i>Method</i>	<i>DOA Indexes</i>			
	ς_1	ψ_1	ς_2	ψ_2
<i>IMSA – SVM</i>				
$s = 1$	8.91	2.33	10.27	3.08
$s = 2$	5.90	0.54	8.46	0.82
$s = S_{opt} = 3$	4.55	0.23	3.90	0.25
<i>Bare SVM</i>	6.04	0.67	16.78	3.78
<i>MLP</i>	17.54	0.27	30.53	2.21
<i>RBF</i>	17.19	0.28	27.77	0.99

Tab. III - M. Donelli *et al.*, “An Innovative Multi-Resolution Approach...”

	<i>DOA Indexes</i>					
<i>Method</i>	ς_1	ψ_1	ς_2	ψ_2	ς_3	ψ_3
<i>IMSA – SVM</i>						
$s = 1$	5.50	0.2	5.59	1.43	4.61	1.56
$s = 2$	4.15	0.06	5.42	0.74	4.43	0.55
$s = S_{opt} = 3$	4.24	0.009	5.19	0.33	3.10	0.14
<i>Bare SVM</i>	10.11	0.35	4.34	1.44	16.52	1.55
<i>MLP</i>	2.45	0.6	21.77	1.09	22.82	2.36
<i>RBF</i>	28.31	1.35	37.34	0.49	29.57	0.67

Tab. IV - M. Donelli et al., “An Innovative Multi-Resolution Approach...”

<i>Method</i>	<i>DOA Indexes</i>							
	ς_1	ψ_1	ς_2	ψ_2	ς_3	ψ_3	ς_4	ψ_4
<i>IMSA – SVM</i>								
$s = 1$	6.84	0.40	24.37	0.40	23.31	1.48	25.47	1.56
$s = 2$	5.85	0.31	28.01	0.31	16.96	0.91	8.08	0.68
$s = S_{opt} = 3$	3.44	0.16	29.33	0.16	12.31	0.21	7.42	0.24
<i>Bare SVM</i>	8.37	2.89	24.71	2.89	26.52	2.89	25.68	2.89
<i>MLP</i>	38.98	0.52	8.91	0.52	35.34	1.82	17.46	1.69
<i>RBF</i>	15.19	0.32	18.69	0.32	40.65	1.81	22.01	0.91

Tab. V - M. Donelli et al., “An Innovative Multi-Resolution Approach...”

<i>Method</i>	<i>DOA Indexes</i>							
	ς_1	ψ_1	ς_2	ψ_2	ς_3	ψ_3	ς_4	ψ_4
<i>IMSA – SVM</i>								
$s = 1$	15.50	0.89	11.51	0.89	45.50	2.98	57.71	2.98
$s = 2$	12.78	0.39	10.65	0.39	10.80	0.72	24.12	0.72
$s = S_{opt} = 3$	12.91	0.16	10.55	0.16	4.71	0.26	17.01	0.26
<i>Bare SVM</i>	15.46	0.91	11.64	0.91	46.53	3.17	58.66	3.17
<i>MLP</i>	9.35	0.29	8.66	0.29	13.75	1.75	27.43	1.75
<i>RBF</i>	8.06	0.26	8.77	0.26	14.84	0.57	9.50	0.57

Tab. VI - M. Donelli *et al.*, “An Innovative Multi-Resolution Approach...”

<i>Method</i>	<i>DOA Indexes</i>							
	ς_1	ψ_1	ς_2	ψ_2	ς_3	ψ_3	ς_4	ψ_4
<i>IMSA – SVM</i>								
$s = 1$	16.98	0.88	39.13	2.81	54.57	2.81	64.78	2.81
$s = 2$	16.51	0.62	6.04	1.70	22.43	1.70	35.70	1.70
$s = S_{opt} = 3$	8.13	0.59	6.18	1.46	11.84	1.46	28.89	1.46
<i>Bare SVM</i>	17.38	0.87	39.45	2.85	54.87	2.85	65.72	2.85
<i>MLP</i>	11.62	0.19	27.46	1.08	11.41	1.08	8.15	1.08
<i>RBF</i>	6.51	0.10	16.85	0.10	3.01	0.10	20.63	0.10

Tab. VII - M. Donelli *et al.*, “An Innovative Multi-Resolution Approach...”

<i>Method</i>	<i>DOA Indexes</i>	
	$\hat{\xi}$	$\hat{\psi}$
<i>IMSA – SVM</i>	1.20	0.21
<i>Bare SVM</i>	2.82	1.94
<i>MLP</i>	13.78	1.66
<i>RBF</i>	13.62	1.21

Tab. VIII - M. Donelli *et al.*, “An Innovative Multi-Resolution Approach...”